Properties of Building Materials

9

V.K.R. Kodur and T.Z. Harmathy

Introduction

Building components are to be designed to satisfy the requirements of serviceability and safety limit states. One of the major safety requirements in building design is the provision of appropriate fire resistance to various building components. The basis for this requirement can be attributed to the fact that, when other measures of containing the fire fail, structural integrity is the last line of defense. In this chapter, the term *structural member* is used to refer to both load-bearing (e.g., columns, beams, slabs) and non-load-bearing (e.g., partition walls, floors) building components.

Fire resistance is the duration during which a structural member exhibits resistance with respect to structural integrity, stability, and temperature transmission. Typical fire resistance rating requirements for different building components are specified in building codes.

In the past, the fire resistance of structural members could be determined only by testing. In recent years however, the use of numerical methods for the calculation of the fire resistance of various structural members is gaining acceptance because these calculation methods are far less costly and time consuming. The fire performance of a structural member depends, in part, on the properties of the materials the building component is composed of. The availability of material properties at high temperature and temperature distributions permits a mathematical approach to predicting the performance of building components exposed to fire. When a structural member is subjected to a defined temperature-time exposure during a fire, this exposure will cause a predictable temperature distribution in the member. Increased temperatures cause deformations and property changes in the materials. With knowledge of the deformations and property changes, the usual methods of structural mechanics can be applied to predict fire resistance performance.

In recent years, significant effort has been undertaken to develop material properties of various construction materials at elevated temperatures. In this chapter, the characteristics of materials are outlined. The various properties that influence fire resistance performance, together with the methods used to develop these properties, is discussed. The trends on the variation of thermal, mechanical, and other material-specific properties with temperature of commonly used construction materials are presented.

Material Characteristics

Classification

Materials, based on composition, can be classified as either a homogeneous or heterogeneous type.

V.K.R. Kodur (✉)
Civil and Environmental Engineering, Michigan State University, East Lansing, Michigan, USA

T.Z. Harmathy

M. Hurley (ed.), *SFPE Handbook of Fire Protection Engineering*,
DOI 10.1007/978-1-4939-2565-0_9,

Homogeneous materials have the same composition and properties throughout their volume and are rarely found in nature. *Heterogeneous* materials have different composition and properties. Most construction materials are heterogeneous, yet their heterogeneity is often glossed over when dealing with practical problems.

The heterogeneity of concrete is easily noticeable. Other heterogeneities related to the microstructure of materials, that is, their grain and pore structures, are rarely detectable by the naked eye. The microstructure depends greatly on the way the materials are formed. In general, materials formed by solidification from a melt show the highest degree of homogeneity. The result of the solidification is normally a *polycrystalline* material, comprising polyhedral grains of crystals, which, in general, are equiaxial and randomly oriented. Severe cold working in metals may produce an elongated grain structure and crystals with preferred orientations.

Noncrystalline solids are called *amorphous* materials. Gels and glasses are amorphous materials. Gels are formed by the coagulation of a colloidal solution. Glasses (vitreous materials) are solids with a liquid-like, grainless submicroscopic structure with low crystalline order. On heating, they will go through a series of phases of decreasing viscosity.

Synthetic polymers (plastics) are made up of long macromolecules created by polymerization from smaller repeating units (monomers). In the case of *thermoplastic* materials, the mobility of the molecular chains increases on heating. Such materials soften, much like glass. In some other types of plastics, called *thermosetting* materials, polymerization also produces cross-bonds between the molecular chains. These cross-bonds prevent the loosening of the molecular structure and the transition of the material into a liquid-like state.

Some building materials (e.g., gypsum, brick) are formed from a wet, plastic mass or from compacted powders by firing. The resulting product is a polycrystalline solid with a well-developed pore structure. Two important building materials, concrete and gypsum, are formed by mixing finely ground powders (and aggregates) with water. The mixture solidifies by hydration. The cement paste in a concrete has a highly complex microstructure, interspersed with very fine, elaborate pores.

Most building materials can be treated as *isotropic* materials, that is, as though they possessed the same properties in all directions. An exception to this is some of the advanced composite materials, such as fiber-reinforced polymers (FRP), which might possess varying properties in different directions and are classified as *anisotropic* materials.

Among the material properties, those that are unambiguously defined by the current composition and phase are referred to as *structure-insensitive*. Some others depend on the microstructure of the solid or on its previous history. These properties are *structure-sensitive*.

Porosity and Moisture Sorption

The fire performance of a material is dependent on the chemical composition and molecular structure of the material. The presence of water in the material composition influences the properties of materials at elevated temperatures. The two commonly associated terms to describe the composition and the extent of water present in a material are porosity and moisture sorption.

What is commonly referred to as a solid object is actually all the material within its visible boundaries. Clearly, if the solid is porous—and most building materials are—the so-called solid consists of at least two phases: (1) a solid-phase matrix and (2) a gaseous phase (namely, air) in the pores within the matrix. Usually, however, there is also a liquid or liquid-like phase present: moisture either absorbed from the atmosphere to the pore surfaces or held in the pores by capillary condensation. This third phase is always present if the pore structure is continuous; discontinuous pores (like the pores of some foamed plastics) are not readily accessible to atmospheric moisture.

The pore structure of materials is characterized by two properties: *porosity, P* ($m^3 \cdot m^{-3}$), the volume fraction of pores within the visible boundaries of the solid; and *specific surface, S* ($m^2 \cdot m^{-3}$), the surface area of the pores per unit volume of the material. For a solid with

continuous pore structure, the porosity is a measure of the maximum amount of water the solid can hold when saturated. The specific surface and (to a lesser degree) porosity together determine the moisture content the solid holds in equilibrium with given atmospheric conditions.

The *sorption isotherm* shows the relationship at constant temperature between the equilibrium moisture content of a porous material and the relative humidity of the atmosphere. A sorption isotherm usually has two branches: (1) an *adsorption branch,* obtained by monotonically increasing the relative humidity of the atmosphere from 0 to 100 % through very small equilibrium steps; and (2) a *desorption branch,* obtained by monotonically lowering the relative humidity from 100 to 0 %. Derived experimentally, the sorption isotherms offer some insight into the nature of the material's pore structure [1, 2].

For heterogeneous materials consisting of solids of different sorption characteristics (e.g., concrete, consisting of cement paste and aggregates), the sorption isotherms can be estimated using the simple mixture rule (with $m = 1$; see Equation 9.1).

Building materials, such as concrete (or more accurately, the cement paste in the concrete) and wood, because of their large specific surfaces, can hold water in amounts substantial enough to be taken into consideration in fire performance assessments.

Mixture Rules

Some properties of materials of mixed composition or mixed phase can be calculated by simple rules if the material properties for the constituents are known. The simplest mixture rule is [3]

$$\pi^m = \sum_i v_i \pi_i^m \tag{9.1}$$

where

π = Material property for the composite

π_i = Material property for the composite's ith constituent

v_i ($m^3 \cdot m^{-3}$) = Volume fraction of the ith constituent

m (dimensionless) = Constant that has a value between −1 and +1

Hamilton and Crosser recommended the following rather versatile formula for two-phase solids [4]:

$$\pi = \frac{v_1 \pi_1 + \gamma v_2 \pi_2}{v_1 + \gamma v_2} \tag{9.2}$$

where

$$\gamma = \frac{n \pi_1}{(n-1)\pi_1 + \pi_2} \tag{9.3}$$

Here phase 1 must always be the principal continuous phase. n (dimensionless) is a function of the geometry of phase distribution. With $n \to \infty$ and $n = 1$, Equations 9.2 and 9.3 convert into Equation 9.1 with $m = 1$ and $m = -1$, respectively. With $n = 3$, a relation is obtained for a two-phase system where the discontinuous phase consists of spherical inclusions [5].

By repeated application, Equations 9.2 and 9.3 can be extended to a three-phase system [6], for example, to a moist, porous solid that consists of three essentially continuous phases (the solid matrix, with moisture and air in its pores).

Survey of Building Materials

There are burnable (combustible) and nonburnable (noncombustible) building materials. The reason for preferring the use of the words *burnable* and *nonburnable* has been discussed by Harmathy [2]. To a designer concerned with the structural performance of a building during a fire, the mechanical and thermal properties of these materials are of principal interest. Yet burnable building materials may become ignited, and thereby the positive role assigned to these materials by design (i.e., functioning as structural elements of the building) may change into a negative role—that is, becoming fuel and adding to the severity of fire. Those properties of burnable building materials that are related to the latter role are discussed in other chapters of this handbook.

From the point of view of their performance in fire, building materials can be divided into the following groups:

1. *Group L (load-bearing) materials*. Materials capable of carrying high stresses, usually in tension or compression. With these materials, the mechanical properties related to behavior in tension and/or compression are of principal interest.
2. *Group L/I (load-bearing/insulating) materials*. Materials capable of carrying moderate stresses and, in fire, providing thermal protection to Group L materials. With Group L/I materials, the mechanical properties (related mainly to behavior in compression) and the thermal properties are of equal interest.
3. *Group I (insulating) materials*. Materials not designed to carry load. Their role in fire is to resist the transmission of heat through building elements and/or to provide insulation to Group L or Group L/I materials. With Group I materials, only the thermal properties are of interest.
4. *Group L/I/F (load-bearing/insulating/fuel) materials*. Group L/I materials that may become fuel in fire.
5. *Group I/F (insulating/fuel) materials*. Group I materials that may become fuel in fire.

The number of building materials has been increasing dramatically during the past few decades. In the last decade or so, a number of high-performing materials, such as FRP and high-strength concrete (HSC), have been developed to achieve cost-effectiveness in construction. Although many of these high-performing materials possess superior properties at ambient temperatures, the same cannot be said of their performance at elevated temperatures. In materials such as HSC, additional complexities such as spalling arise, which may severely impact the fire performance of a structural member.

By necessity, only a few of those materials that are commonly used will be discussed in this chapter in some detail. These materials are as follows: in Group L—structural steel, light-gauge steel, and reinforcing/prestressing steel; Group L/I—concrete and brick (including fiber-reinforced concrete); Group L/I/F (or Group I/F and L/F)—wood and FRP; and Group I—gypsum and insulation.

Material Properties at Elevated Temperatures

The behavior of a structural member exposed to fire is dependent, in part, on the thermal and mechanical properties of the material of which the member is composed. While calculation techniques for predicting the process of deterioration of building components in fire have developed rapidly in recent years, research related to supplying input information into these calculations has not kept pace. The designer of the fire safety features of buildings will find that information on the properties of building materials in the temperature range of interest, 20–800 °C is not easy to come by. Most building materials are not stable throughout this temperature range. On heating, they undergo physicochemical changes ("reactions" in a generalized sense), accompanied by transformations in their microstructure and changes in their properties. For example, concrete at 500 °C is completely different from the material at room temperature.

The thermophysical and mechanical properties of most materials change substantially within the temperature range associated with building fires. In the field of fire science, applied materials research faces numerous difficulties. At elevated temperatures, many building materials undergo physicochemical changes. Most of the properties are temperature dependent and sensitive to testing method parameters such as heating rate, strain rate, temperature gradient, and so on. Harmathy [7] cited the lack of adequate knowledge of the behavior of building materials at elevated temperatures as the most disturbing trend in fire safety engineering. There has been a tendency to use "notional" (also called "typical," "proprietary," "empirical," etc.) values for material properties in numerical computations—in other words, values that ensure agreement between experimental and analytical results. Harmathy warned that this practice might lead

to a proliferation of theories that lack general validity.

Clearly, the generic information available on the properties of building materials at room temperature is seldom applicable in fire safety design. It is imperative, therefore, that the fire safety practitioner knows how to extend, based on a priori considerations, the utility of the scanty data that can be gathered from the technical literature. Also, knowledge of unique material-specific characteristics at elevated temperatures, such as spalling in concrete or charring in wood, is critical to determine the fire performance of a structural member. These properties are discussed in the following sections.

Reference Condition

Most building materials are porous and therefore capable of holding moisture, the amount of which depends on the atmospheric conditions. Because the presence of moisture may have a significant and often unpredictable effect on the properties of materials at any temperature below 100 °C, it is imperative to conduct all property tests on specimens brought into a moistureless "reference condition" by some drying technique prior to the test. The reference condition is normally interpreted as that attained by heating the test specimen in an oven at 105 °C until its weight shows no change. A few building materials however, among them all gypsum products, may undergo irreversible physicochemical changes when held at that temperature for an extended period. To bring them to a reference condition, specimens of these materials should be heated in a vacuum oven at some lower temperature level (e.g., at 40 °C in the case of gypsum products).

Mechanical Properties

The mechanical properties that determine the fire performance of structural members are strength, modulus of elasticity, and creep of the component materials at elevated temperatures.

Stress-Strain Relationships

The mechanical properties of solids are usually derived from conventional tensile or compressive tests. The strength properties are usually expressed in stress-strain relations, which are often used as input data in mathematical models calculating the fire resistance. Figure 9.1 shows, for a metallic material, the variation of stress, σ (Pa), with increasing strain (deformation), ε ($m \cdot m^{-1}$), while the material is strained (deformed) in a tensile test at a more or less constant rate (i.e., constant crosshead speed), usually of the order of 1 $mm \cdot min^{-1}$. Generally, because of a decrease in the strength and ductility of the material, the slope of the stress-strain curve decreases with increasing temperature.

Modulus of Elasticity, Yield Strength, Ultimate Strength

The modulus of elasticity is a measure of the ability of the material to resist deformation and is expressed as the ratio of the deforming stress to the strain in the material. Generally, the modulus of elasticity of a material decreases gradually with increasing temperature.

The tensile or compressive strength of the material is generally expressed by means of yield strength and ultimate strength. Often the

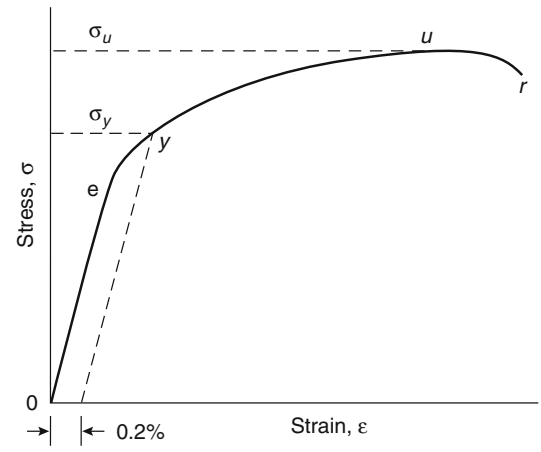

Fig. 9.1 Stress-strain curve (strain rate is roughly constant)

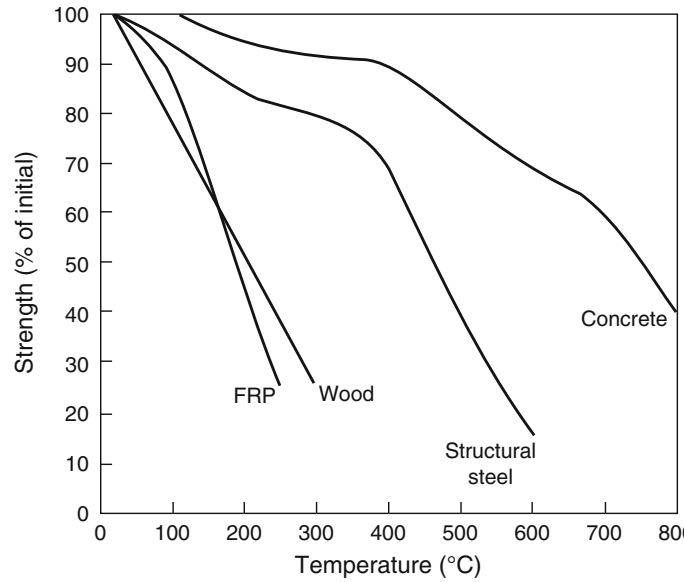

Fig. 9.2 Variation of strength with temperature for different materials

strength at elevated temperature is expressed as a percentage of the compressive (tensile) strength at room temperature. Figure 9.2 shows the variation of strength with temperature (ratio of strength at elevated temperature to that at room temperature) for concrete, steel, wood, and FRP. For all four materials, the strength decreases with increasing temperature; however, the rate of strength loss is different.

For materials such as concrete, compressive strength is of main interest because it has very limited tensile strength at higher temperatures. However, for materials such as steel, both compressive and tensile strengths are of equal interest.

Section 0-*e* of the curve in Fig. 9.1 represents the elastic deformation of the material, which is instantaneous and reversible. The modulus of elasticity, E (Pa), is the slope of that section. Between points *e* and *u* the deformation is plastic, nonrecoverable, and quasi-instantaneous. The plastic behavior of the material is characterized by the yield strength at 0.2 % offset, σ_y (Pa), and the ultimate strength, σ_u (Pa). After some localized necking (i.e., reduction of cross-sectional area), the test specimen ruptures at point *r*. The modulus of elasticity is more or less a structure-insensitive property.

For metals of similar metallurgical characteristics, the stress-strain curve can be reproduced at room temperature at a reasonable tolerance, and the shape of the curve does not depend significantly on the crosshead speed. At sufficiently high temperatures, however, the material undergoes plastic deformation even at constant stress, and the *e*-*r* section of the stress-strain curve will depend markedly on the crosshead speed.

Creep

Creep, often referred to as creep strain, is defined as the time-dependent plastic deformation of the material and is denoted by ε_t ($\mathrm{m \cdot m^{-1}}$). At normal stresses and ambient temperatures, the deformation due to creep is not significant. At higher stress levels and at elevated temperatures, however, the rate of deformation caused by creep can be substantial [8]. Hence, the main factors that influence creep are the temperatures, the stress level, and their duration.

In a creep test the variation of ε_t is recorded against time, t (h), at constant stress (more accurately, at constant load) and at constant (elevated) temperature T (K). A typical strain-time

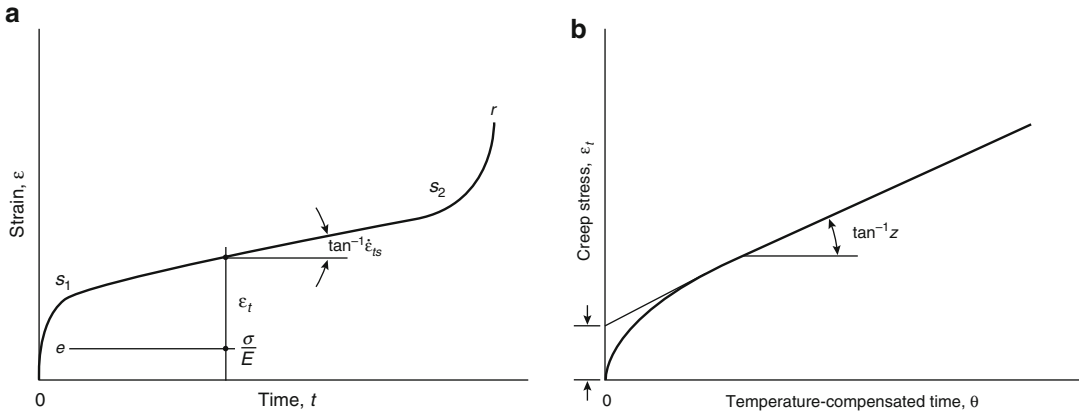

Fig. 9.3 (**a**) Creep strain vs. time curve (T = constant; σ ≈ constant); (**b**) creep strain vs. temperature-compensated time curve (σ ≈ constant)

curve is shown in Fig. 9.3a. The total strain, ε (m·m^{-1}), is

$$\varepsilon = \frac{\sigma}{E} + \varepsilon_t \tag{9.4}$$

The 0-*e* section of the strain-time curve represents the instantaneous elastic (and reversible) part of the curve; the rest is creep, which is essentially nonrecoverable. The creep is fast at first (primary creep, section *e*-s_1 in Fig. 9.3a, then proceeds for a long time at an approximately constant rate (secondary creep, section s_1-s_2), and finally accelerates until rupture occurs (tertiary creep, section s_2-*r*). The curve becomes steeper if the test is conducted either at a higher load (stress) or at a higher temperature.

Dorn's concept is particularly suitable for dealing with deformation processes developing at varying temperatures [9]. Dorn eliminated the temperature as a separate variable by the introduction of a new variable: the "temperature-compensated time," θ (h), defined as

$$\theta = \int_0^t e^{-\Delta H_c/RT} dt \tag{9.5}$$

where ΔHc (J·kmol^{-1}) is the activation energy of creep, and R (J·kmol^1·K^{-1}) is the gas constant.

From a practical point of view, only the primary and the secondary creeps are of importance. It has been shown that the creep strain in these two regimes can be satisfactorily described by the following equation [10]

$$\varepsilon_t = \frac{\varepsilon_{t0}}{\ln 2} \cosh^{-1}\left(2^{Z\theta/\varepsilon_{t0}}\right) \quad (\sigma \simeq \text{constant}) \tag{9.6}$$

or approximated by the simple formula [11]

$$\varepsilon_t \approx \varepsilon_{t0} + Z\theta \quad (\sigma \simeq \text{constant}) \tag{9.7}$$

where Z (h^{-1}) is the Zener-Hollomon parameter, and ε_{t0} (mm^{-1}) is another creep parameter, the meaning of which is explained in Fig. 9.3b. The Zener-Hollomon parameter is defined as [12]

$$Z = \dot{\varepsilon}_{ts} e^{\Delta H/RT} \tag{9.8}$$

where $\dot{\varepsilon}_{ts}$ (mm^{-1}·h^{-1}) is the rate of secondary creep at a temperature, T. The two creep parameters, Z and ε_{t0}, are functions of the applied stress only (i.e., they are independent of the temperature).

For most materials, creep becomes noticeable only if the temperature is higher than about one-third of the melting temperature (on the absolute scale).

The creep of concrete is due to the presence of water in its microstructure [13]. There is no satisfactory explanation for the creep of concrete at elevated temperatures. Anderberg and Thelandersson [14], and Schneider [15] suggested techniques for the calculation of the deformation of concrete under conditions characteristic of fire exposure.

Thermal Properties

The material properties that influence the temperature rise and distribution in a member are its thermal conductivity, thermal expansion, specific heat, thermal diffusivity, and mass loss. These properties depend on the composition and characteristics of the constituent materials.

Thermal Expansion

The thermal expansion characterizes the expansion (or shrinkage) of a material caused by heating and is defined as the expansion (shrinkage) of unit length of a material when it is raised 1° in temperature. The expansion is considered to be positive when the material elongates and is considered negative when it shortens. In general, the thermal expansion of a material is dependent on the temperature. The dilatometric curve is a record of the fractional change of a linear dimension of a solid at a steadily increasing or decreasing temperature. With mathematical symbolism, the dilatometric curve is a plot of

$$\frac{\Delta \ell}{\ell_0} \text{ against T}$$

where $\Delta \ell = \ell - \ell_0$ and ℓ_0 (m) and ℓ (m) are the changed and original dimensions of the solid, respectively, the latter usually taken at room temperature. $\Delta \ell$ reflects not only the linear expansion or shrinkage of the material, but also the dimensional effects brought on by possible physicochemical changes (i.e., "reactions").

The heating of the solid usually takes place at a predetermined rate, 5 °C·min^{-1} as a rule. Because the physicochemical changes proceed at a finite rate and some of them are irreversible, a dilatometric curve obtained by heating rarely coincides with that obtained during the cooling cycle. Sluggish reactions may bring about a steady rise or decline in the slope of the dilatometric curve. Discontinuities in the slope indicate very fast reactions. Heating the material at a rate higher than 5 °C·min^{-1} usually causes the reactions to shift to higher temperatures and to develop faster.

The coefficient of linear thermal expansion, β (m·m^{-1}·K^{-1}), is defined as

$$\beta = \frac{1}{\ell} \frac{d\ell}{dT} \tag{9.9}$$

Since $\ell = \ell_0$ the coefficient of linear thermal expansion is, for all intents, the tangent to the dilatometric curve. For solids that are isotropic in a macroscopic sense, the coefficient of volume expansion is approximately equal to 3β.

The thermal expansion is measured with a dilatometric apparatus, capable of producing curves that show the expansion of the materials with temperature in the range from 20 to 1000 °C. Harmathy [7, 16], using a horizontal dilatometric apparatus, recorded dilametric curves for various types of concrete and brick, some of which are presented in later sections. The sample was 76.2 mm long and about 13 by 13 mm in cross section. It was subjected to a small spring load that varied during the test. Unfortunately, even this small load caused creep shrinkage with those materials that tended to soften at higher temperatures. Furthermore, because the apparatus did not provide a means for placing the sample in a nitrogen atmosphere, in certain cases oxidation may also have had some effect on the shape of the curves.

Mass Loss

The mass loss is often used to express the loss of mass at elevated temperatures. The thermogravimetric curve is a record of the fractional variation of the mass of a solid at steadily increasing or decreasing temperature. Again, with mathematical symbolism, a thermogravimetric curve is a plot of

$$\frac{M}{M_0} \text{ against } T$$

where M and M_0 (kg) are the changed and original masses of the solid, respectively, the latter usually taken at room temperature.

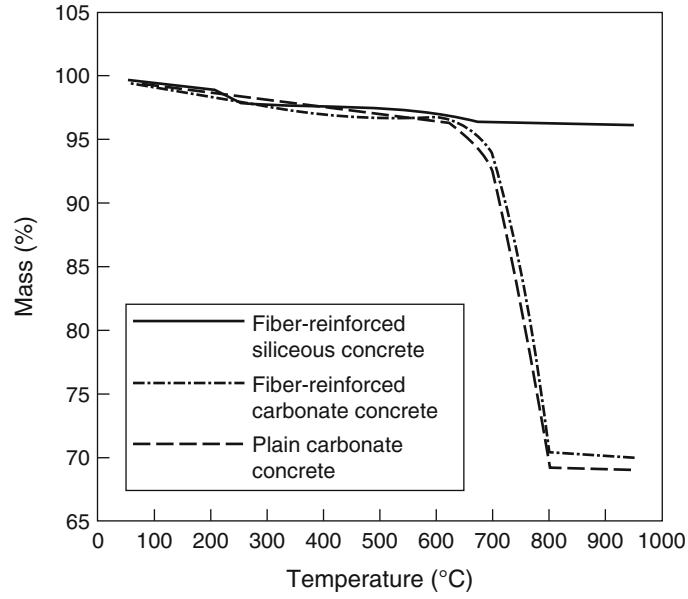

Fig. 9.4 Mass loss of various concrete types as a function of temperature [18]

Generally a heating rate of 5 °C·min^{-1} is used in the measurements.

A thermogravimetric curve reflects reactions accompanied by loss or gain of mass but, naturally, it does not reflect changes in the materials' microstructure or crystalline order. $M/M_0 = 1$ is the thermogravimetric curve for a chemically inert material. Again, an increase in the rate of heating usually causes those features of the curve that are related to chemical reactions to shift to higher temperatures and to develop faster.

The thermogravimetric curves to be shown were obtained by a DuPont 951 thermogravimetric analyzer [17], using specimens of 10–30 mg in mass, placed in a nitrogen atmosphere [7]. The rate of temperature rise was 5 °C·min^{-1}. Figure 9.4 shows the variation of mass loss for concrete in the temperature range from 20 to 1000 °C.

Density, Porosity

The density, ρ (kg·m^{-3}), in an oven-dry condition, is the mass of a unit volume of the material, comprising the solid itself and the air-filled pores. Assuming that the material is isotropic with respect to its dilatometric behavior, its density at any temperature can be calculated from the thermogravimetric and dilatometric curves.

$$\rho = \rho_0 \frac{(M/M_0)_T}{\left[1 + ((\Delta \ell)/(\ell_0))_T\right]} \tag{9.10}$$

where ρ_0 (kg·m^{-3}) is the density of the solid at the reference temperature (usually room temperature), and the T subscript indicates values pertaining to temperature T in the thermogravimetric and dilatometric records.

The density of composite solids at room temperature can be calculated by means of the mixture rule in its simplest form (Equation 9.1 with $m = 1$).

$$p = \sum_i v_i p_i \tag{9.11}$$

where the i subscript relates to information on the ith component. At elevated temperatures, the expansion of the components is subject to constraints, and therefore the mixture rule can yield only a crude approximation.

If, as usual, the composition is given in mass fractions rather than in volume fractions, the volume fractions can be obtained as

$$v_i = \frac{w_i / p_i}{\sum_i w_i / p_i} \tag{9.12}$$

where w_i is the mass fraction of the ith component (kg·kg^{-1}).

True density, ρ_t (kg·m^{-3}), is the density of the solid in a poreless condition. Such a condition is nonexistent for many building materials and, therefore, may be a theoretical value derived on crystallographic considerations, or determined by some standard technique, for example, ASTM C135 [19]. The relationship between the porosity and density is

$$P = \frac{\rho_t - \rho}{\rho_t} \tag{9.13}$$

The overall porosity of a composite material consisting of porous components is

$$P = \sum_i v_i P_i \tag{9.14}$$

where, again, the i subscript relates to the ith component of the material.

Specific Heat

The specific heat of a material is the characteristic that describes the amount of heat required to raise a unit mass of the material at unit temperature. A calorimetric curve describes the variation with temperature of the apparent specific heat of a material at constant pressure, cp (J·kg^{-1}·K^{-1}). The apparent specific heat is defined as

$$c_p = \frac{\delta h}{\delta T_p} \tag{9.15}$$

where h is enthalpy (J·kg^{-1}), and the p subscripts indicate the constancy of pressure. If the heating of the solid is accompanied by physicochemical changes (i.e., "reactions"), the enthalpy becomes a function of the reaction progress variable, ξ (dimensionless), that is, the degree of conversion at a particular temperature from reactant(s) into product(s). For any temperature interval where physicochemical change takes place [2, 6, 20], $0 \leq \xi \leq 1$, and

$$c_p = \overline{c}_p + \Delta h \frac{d\xi}{dT} \tag{9.16}$$

where cp (J·kg^{-1}·K^{-1}) is the specific heat for that mixture of reactants and (solid) products that the material consists of at a given stage of the conversion (as characterized by ξ), and $\Delta\, hp$ (J·kg^{-1}) is the latent heat associated with the physicochemical change.

As Equation 9.16 and Fig. 9.5 show, in temperature intervals of physicochemical instability, the apparent specific heat consists of sensible heat and latent heat contributions. The latter contribution will result in extremities in the calorimetric curve: a maximum if the reaction is endothermic, a minimum if it is exothermic.

In heat flow studies, it is usually the ρcp product (J·m^{-3}·K^{-1}) rather than cp that is needed as input information. This product is referred to as volume specific heat.

Until the 1980s, adiabatic calorimetry was the principal method to study the shape of the cp versus T relationship. Since the 1980s, differential scanning calorimetry (DSC) has been the most commonly used technique for mapping the curve in a single temperature sweep at a desired rate of heating. Unfortunately, the accuracy of the DSC technique in determining the sensible heat contribution to the apparent specific heat may not be particularly good (sometimes it may be as low as ±20 %). The rate of temperature rise was usually 5 °C·min^{-1}. At higher heating rates, the peaks in the DSC curves tend to shift to higher

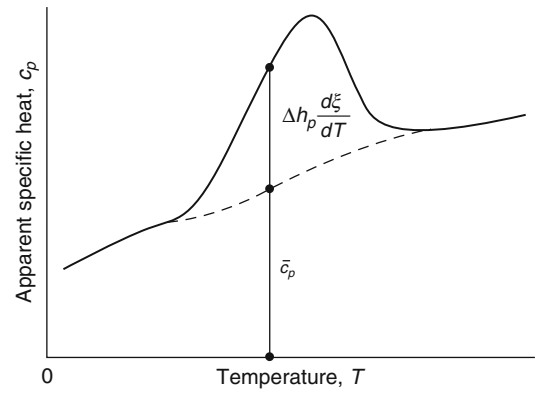

Fig. 9.5 The apparent specific heat

temperatures and become sharper. For temperatures above 600 °C, a high-temperature differential thermal analyzer (DTA) is also used. Harmathy, with the aid of a DuPont 910 differential scanning calorimeter, developed calorimetric curves for a number of materials by placing the samples, 10–30 mg in mass, in a nitrogen atmosphere [7, 21].

Materials that undergo exothermic reactions may yield negative values in the calorimetric curve. A negative value for *cp* indicates that, at the applied (and enforced) rate of heating, the rate of evolution of reaction heat exceeds the rate of absorption of sensible heat by the material. In natural processes, the apparent specific heat can never be negative, because the heat evolving from the reaction is either scattered to the surroundings or, if absorbed by the material, causes a very fast temperature rise. If the heat of reaction is not very high, obtaining nonnegative values for *cp* can be achieved by suitably raising the scanning rate. For this reason, some materials undergoing exothermic reactions must be tested at rates of heating higher than 5 °C·min^{-1}, often as high as 50 °C·min^{-1}.

If experimental information is not available, the *cp* versus *T* relationship can be calculated from data on heat capacity and heat of formation for all the components of the material (including reactants and products), tabulated in a number of handbooks [22, 23]. Examples of calculations are presented in Harmathy [2, 6], where information is developed for the apparent specific heat versus temperature relation for a cement paste and four kinds of concrete.

Thermal Conductivity

The temperature rise in a member, as a result of heat flow, is a function of the thermal conductivity of the material. Heat transmission solely by conduction can occur only in poreless, nontransparent solids. In porous solids (most building materials), the mechanism of heat transmission is a combination of conduction, radiation, and convection. (If pore size is less than that about 5 mm, the contribution of pores to convective heat transmission is negligible.) The thermal conductivity of porous materials is, in a strict sense, merely a convenient empirical factor that makes it possible to describe the heat transmission process with the aid of the Fourier law. That empirical factor will depend not only on the conductivity of the solid matrix but also on the porosity of the solid and the size and shape of the pores. At elevated temperatures, because of the increasing importance of radiant heat transmission through the pores, conductivity becomes sensitive to the temperature gradient.

Because measured values of the thermal conductivity depend to some extent on the temperature gradient employed in the test, great discrepancies may be found in thermal conductivity data reported by various laboratories. A thermal conductivity value yielded by a particular technique is, in a strict sense, applicable only to heat flow patterns similar to that characteristic of the technique employed.

Experimental data indicate that porosity is not a greatly complicating factor as long as it is not larger than about 0.1. With insulating materials, however, the porosity may be 0.8 or higher. Conduction through the solid matrix may be an insignificant part of the overall heat transmission process; therefore, using the Fourier law of heat conduction in analyzing heat transmission may lead to deceptive conclusions. If the solid is not oven-dry, a temperature gradient will induce migration of moisture, mainly by an evaporation condensation mechanism [24]. The migration of moisture is usually, but not necessarily, in the direction of heat flow and manifests itself as an increase in the apparent thermal conductivity of the solid. Furthermore, even oven-dry solids may undergo decomposition (mainly dehydration) reactions at elevated temperatures. The sensible heat carried by the gaseous decomposition products as they move in the pores adds to the complexity of the heat flow process. At present there is no way of satisfactorily accounting for the effect of simultaneous mass transfer on heat flow processes occurring under fire conditions.

The thermal conductivity of layered, multiphase solid mixtures depends on whether the phases lie in the direction of, or normal to, the direction of heat flow and is determined

using the simple mixture rule [4, 25]. At higher temperatures, because of radiative heat transfer through the pores, the contribution of the pores to the thermal conductivity of the solid must not be disregarded [26].

The thermal conductivity of solids is a structure-sensitive property. For crystalline solids, the thermal conductivity is relatively high at room temperature and gradually decreases as the temperature rises. For predominantly amorphous solids, on the other hand, the conductivity is low at room temperature and increases slightly with the rise of temperature. The conductivity of porous crystalline materials may also increase at very high temperatures because of the radiant conductivity of the pores.

The thermal conductivity of materials such as concrete or brick can be measured, in the temperature range between 20 and 800 °C, using a non-steady-state hot wire method [27, 28]. The thermal conductivity values at discrete temperature levels can be plotted to obtain a curve. Unfortunately, no scanning technique exists for acquiring a continuous thermal conductivity versus temperature curve from a single temperature sweep. Special problems arise with the estimation of the thermal conductivity for temperature intervals of physicochemical instability. Both the steady-state and variable-state techniques of measuring thermal conductivity require the stabilization of a pattern of temperature distribution (and thereby a certain microstructural pattern) in the test sample prior to the test. The test results can be viewed as points on a continuous thermal conductivity versus temperature curve obtained by an imaginary scanning technique performed at an extremely slow scanning rate. Because each point pertains to a more or less stabilized microstructural pattern, there is no way of knowing how the thermal conductivity would vary in the course of a physicochemical process developing at a finite rate and varying microstructure.

On account of the nonreversible microstructural changes brought about by heating, the thermal conductivity of building materials (and perhaps most other materials) is usually different in the heating and cooling cycles. Open and solid circles are used in the figures to identify thermal conductivity values obtained by stepwise increasing and stepwise decreasing the temperature of the sample, respectively. Also, often the thermal conductivity of a material is taken as invariant with respect to the direction of heat flow.

Thermal Diffusivity

The thermal diffusivity of a material is defined as the ratio of thermal conductivity to the volumetric specific heat of the material. It measures the rate of heat transfer from an exposed surface of a material to the inside. The larger the diffusivity, the faster the temperature rise at a certain depth in the material. Similar to thermal conductivity and specific heat, thermal diffusivity varies with temperature rise in the material. Thermal diffusivity, α, can be calculated using the relation

$$\alpha = \frac{k}{\rho c_p} \tag{9.17}$$

where
k = Thermal conductivity
ρ = Density
c_p = Specific heat of the material

Special (Material-Specific) Properties

In addition to thermal and mechanical properties, certain other properties, such as spalling in concrete and charring in wood, influence the performance of a material at elevated temperature. These properties are unique to specific materials and are critical for predicting the fire performance of a structural member.

Critical Temperature

In building materials, such as steel and FRP, the determination of failure in a structural member exposed to fire is simplified to the calculation of critical temperature. The critical temperature is defined as the temperature at which the material

loses much of its strength and can no longer support the applied load. When this temperature is reached, the safety factor against failure becomes less than 1.

North American standards (ASTM E119) assume a critical or failure temperature of 538 °C (1000 °F) for structural steel. It is a typical failure temperature for columns under full design load. This temperature is also regarded as the failure temperature in the calculation of fire resistance of steel members. If a load is applied to the member, the test is continued until the member actually fails, which, depending on the load intensity, may occur at a higher or lower steel temperature.

This concept of critical temperature is also used for reinforced and prestressed steel in concrete structural members for evaluating the fire resistance ratings. These ratings are generally obtained through the provision of minimum member dimensions and minimum thickness of concrete cover. The minimum concrete cover thickness requirements are intended to ensure that the temperature in the reinforcement does not reach its critical temperature for the required duration. For reinforcing steel, the critical temperature is 593 °C, whereas for prestressing steel the critical temperature is 426 °C [29].

Spalling

Spalling is defined as the breaking of layers (pieces) of concrete from the surface of the concrete elements when the concrete elements are exposed to high and rapidly rising temperatures, such as those experienced in fires. Spalling can occur soon after exposure to heat and can be accompanied by violent explosions, or it may happen when concrete has become so weak after heating that, when cracking develops, pieces fall off the surface. The consequences may be limited as long as the extent of the damage is small, but extensive spalling may lead to early loss of stability and integrity due to exposed reinforcement and penetration of partitions.

Although spalling might occur in all concretes, high-strength concrete (HSC) is believed to be more susceptible than normal-strength concrete (NSC) because of its low permeability and low water-cement ratio. In a number of test observations on HSC specimens, it has been found that spalling is often of an explosive nature [30, 31]. Hence, spalling is one of the major concerns in the use of HSC and should be properly accounted for in evaluating fire performance. Spalling in NSC and HSC columns is compared in Fig. 9.6 using the data

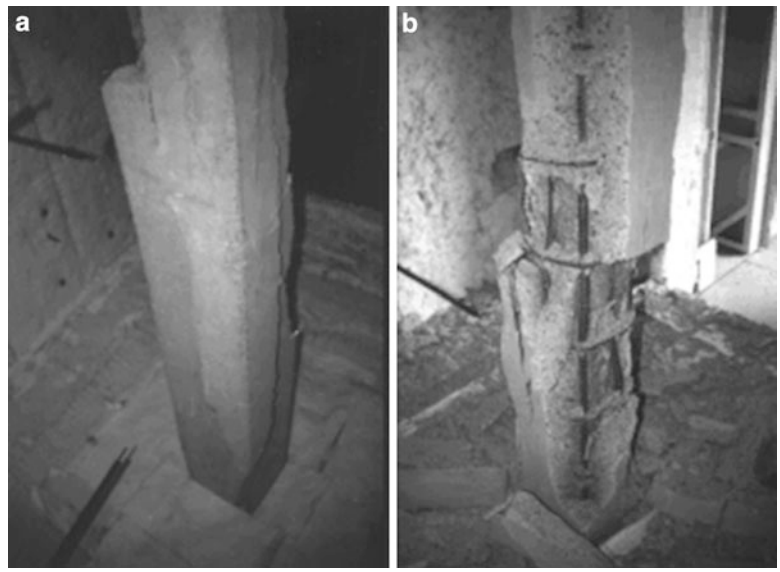

Fig. 9.6 Spalling in NSC and HSC columns after exposure to fire [32]: (**a**) normal-strength concrete column and (**b**) high-strength concrete column

obtained from full-scale fire tests on loaded columns [32]. It can be seen that the spalling is quite significant in the HSC column.

Spalling is believed to be caused by the buildup of pore pressure during heating. The extremely high water vapor pressure, generated during exposure to fire, cannot escape due to the high density (and low permeability) of HSC, and this pressure buildup often reaches the saturation vapor pressure. At 300 °C, the pressure reaches approximately 8 MPa; such internal pressures are often too high to be resisted by the HSC mix having a tensile strength of approximately 5 MPa [33]. The drained conditions at the heated surface, and the low permeability of concrete, lead to strong pressure gradients close to the surface in the form of the so-called "moisture clog." [2, 34] When the vapor pressure exceeds the tensile strength of concrete, chunks of concrete fall off from the structural member. The pore pressure is considered to drive progressive failure; that is, the lower the permeability of concrete, the greater the spalling. This falling off can often be explosive in nature, depending on the fire and concrete characteristics.

However, other researchers explain the occurrence of spalling on the basis of fracture mechanics and state that the spalling results from restrained thermal dilatation close to the heated surface [35]. This leads to compressive stresses parallel to the heated surface, which are released by brittle fractures of concrete, in other words, spalling.

Spalling, which often results in the rapid loss of concrete during a fire, exposes deeper layers of concrete to fire temperatures, thereby increasing the rate of transmission of heat to the inner layers of the member, including the reinforcement. When the reinforcement is directly exposed to fire, the temperatures in the reinforcement rise at a very high rate, leading to a faster decrease in strength of the structural member. The loss of strength in the reinforcement, added to the loss of concrete due to spalling, significantly decreases the fire resistance of a structural member.

In addition to strength and porosity of concrete mix, density, load intensity, fire intensity, aggregate type, and relative humidity are the primary parameters that influence spalling in HSC. The variation of porosity with temperature is an important property needed for predicting spalling performance of HSC. Noumowe et al. carried out porosity measurements on NSC and HSC specimens, using a mercury porosimeter, at various temperatures [36].

Charring

Charring is the process of formation of a layer of char at the exposed surface of wood members during exposure to fire. The charring process also occurs in other members, such as FRP and some types of plastics. When exposed to heat, wood undergoes thermal degradation (pyrolysis), the conversion of wood to char and gas, resulting in a reduction of the density of the wood. Studies have shown that the charring temperature for wood lies in the range of 280–300 °C [29].

The charred layer is considered to have practically no strength. The fire resistance of the member depends on the extent of charring and the remaining strength of the uncharred portion.

The charring rate, a critical parameter in determining the fire resistance of a structural wood member, is defined as the rate at which wood is converted to char. In the standard fire resistance test, it has been noted that the average rate of charring transverse to the grain is approximately 0.6 mm/min [29]. The charring rate parallel to the grain of wood is approximately twice the rate when it is transverse to the grain. Detailed studies on the charring rates for several specimen and timber types are reported by various researchers [37–39] and are summarized in a report [40]. These charring rates were constant (in each study) and ranged from 0.137 to 0.85 mm/min. The assumption of a constant rate of charring is reasonable for thick wood members.

Charring is influenced by a number of parameters, the most important ones being density, moisture content, and contraction of wood. The influence of the moisture content and density of the wood on the charring rate is illustrated in Fig. 9.7 for Douglas fir exposed to the standard

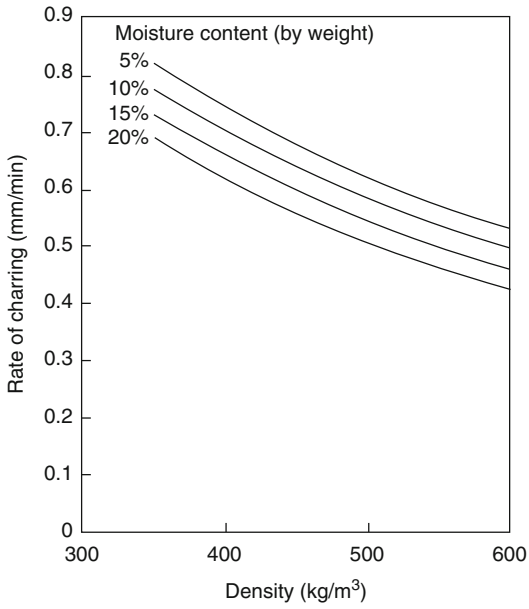

Fig. 9.7 Rate of charring in Douglas fir as a function of its density (dry condition) for various moisture contents when exposed to ASTM standard fire [29]

fire [29]. It can be seen that the charring rate decreases with increasing density of the wood and also with increasing moisture content.

It is important to recognize that the charring rate in real fires depends on the severity of fire to which the wood is exposed. It should be noted that the charring rate is a function of the imposed radiant heat flux. This depends on the fuel load and the ventilation factor of the compartment (for full details see Chap. 30, in this book). Detailed information on the charring of untreated wood—with expressions for charring rate in terms of the influencing factors of density, moisture content, external heat flux, and oxygen concentration—when exposed to real fires is given by Hadvig [41] and Mikkola [42].

Sources of Information

Information on the properties of building materials at elevated temperatures is scattered throughout the literature. There are a few publications, however, that may be particularly valuable for fire safety practitioners. A book by Harmathy [2] and the ASCE manual on structural fire protection [29] present a wealth of information on concrete, steel, wood, brick, gypsum, and various plastics. The thermal properties of 31 building materials are surveyed in an NRCC report [7]. The mechanical and thermal properties of concrete are discussed in an ACI guide [43], and in reports by Bennetts [44] and Schneider [45]. Those of steel are surveyed in the ACI guide, in Bennetts's report, and in a report by Anderberg [46]. Information on the thermal conductivity of more than 50 rocks (potential concrete aggregates) is presented in a paper by Birch and Clark [47]. The relationships for thermal and mechanical properties, at elevated temperatures, for some building materials are listed in the ASCE structural fire protection manual [29]. In most cases these properties are expressed, in the temperature range of 0–1000 °C, as a function of temperature and other properties at ambient temperature. These values can be used as input data in mathematical models for predicting cross sectional temperatures and fire performance of structural members.

Steel

Steel is a Group L material. The steels most often used in the building industry are either hot-rolled or cold-drawn. The structural steels and concrete reinforcing bars are hot-rolled, low-carbon, ferrite-pearlite steels. They have a randomly oriented grain structure, and their strength depends mainly on their carbon content. The prestressing steel wires and strands for concrete are usually made from cold-drawn, high-carbon, pearlitic steels with an elongated grain structure, oriented in the direction of the cold work. In addition, light-gauge steel, made from cold-formed steel, finds wide applications in lightweight framing, such as walls and floors.

Information on the mechanical properties of two typical steels (a structural steel [ASTM A36] and a prestressing wire [ASTM A421]) is presented in Figs. 9.8, 9.9, and 9.10 and in Table 9.1 [48]. Figures 9.8 and 9.9 are stress-strain curves at room temperature (24 °C and

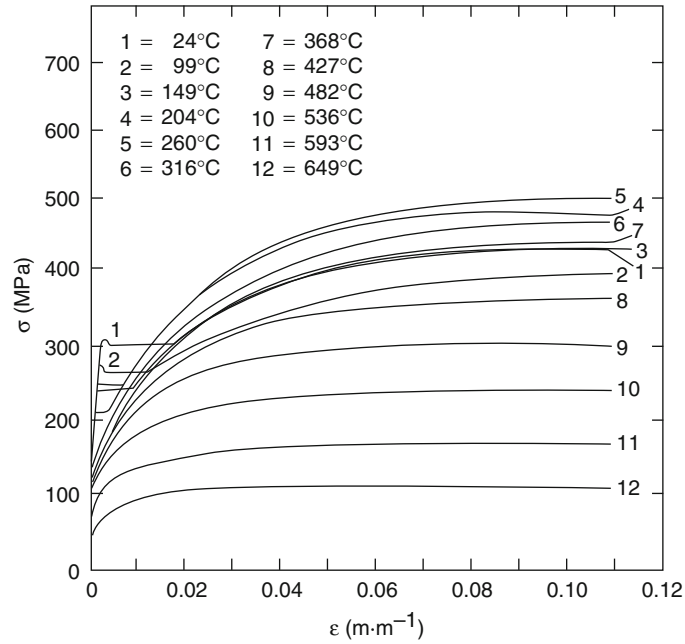

Fig. 9.8 Stress-strain curves for a structural steel (ASTM A36) at room temperature and elevated temperatures [48]

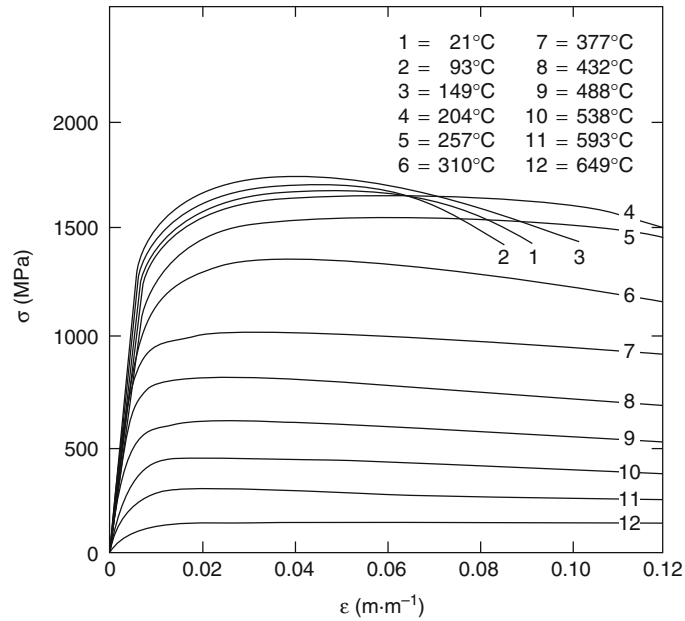

Fig. 9.9 Stress-strain curves for prestressing steel (ASTM A421) at room temperature and elevated temperatures [48]

21 °C, respectively) and at a number of elevated temperature levels. Figure 9.10 shows the effect of temperature on the yield and ultimate strengths of the two steels.

Table 9.1 presents information on the effect of stress on the two creep parameters, Z and ε_{t0} (see Equation 9.7). Because creep is a very structure-sensitive property, the creep parameters may show a substantial spread, even for steels with similar characteristics at room temperature. The application of the creep parameters to the calculation of the time of structural failure in fire is discussed in Hamilton and Crosser [4, 8].

The modulus of elasticity (E) is about 210×10^3 MPa for a variety of common steels at room temperature. Figure 9.11 shows its variation with temperature for structural steels [50] and steel reinforcing bars [49]. (E_0 in Fig. 9.11 is the modulus of elasticity at room temperature.)

The density (ρ) of steel is about 7850 kg·m^{-3}. Its coefficient of thermal expansion (β) is a structure-insensitive property. For an average carbon steel, β is 11.4×10^{-6} m·m^{-1}·K^{-1} at room temperature. The dilatometric curve shown in Fig. 9.12 is applicable to most of the common steels. The curve reveals substantial contraction of the material at about 700 °C, which is associated with the transformation (phase change of steel) of the ferrite-pearlite structure into austenite.

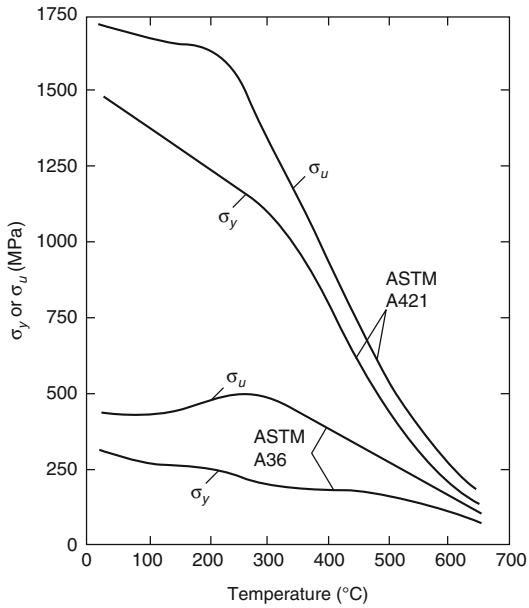

Fig. 9.10 The ultimate and yield strengths for a structural steel (ASTM A36) and a prestressing steel (ASTM A421) at elevated temperatures [48]

Being a structure-sensitive property, the thermal conductivity of steel is not easy to define. For carbon steels it usually varies within the range of 46–65 W·m^{-1}·K^{-1}.

Equations for various properties of steel, as functions of temperature, are available in the ASCE structural fire protection manual [29] and in Eurocode 3 [51, 52]. In the ASCE manual, the same set of relationships is applicable for thermal properties of both structural and reinforcing steel. However, separate relationships for stress-strain and elasticity are given for the two steels with slightly conservative values for structural steel. Recently, Poh proposed a general stress-strain equation that expresses stress explicitly in terms of strain in a single continuous curve [53, 54].

The critical temperature of steel is often used as a benchmark for determining the failure of structural members exposed to fire. This ensures that the yield strength is not reduced to less than that of 50 % of ambient value. The critical temperature for various types of steels is given in Table 9.2.

The above discussed high temperature properties are generally applicable to conventional carbon (mild) steel whose chemical composition consist of iron, carbon, manganese, sulfur and phosphorous. In recent years, a number of new steels are available and these steel are made by adding alloys, such as nickel, titanium, boron and chromium. These alloys influence durability characteristics, as well mechanical properties of steel. For example, molybdenum, chromium and niobium can increase the fire resistance property of steel, while chrome and nickel can enhance the corrosion resistance of steel [56]. Current design rules on fire resistance of steel structures (EC3 2005b [51], BS:5950

Table 9.1 Creep parameters for a structural steel and a prestressing steel [48]

Steel	$\Delta H_c/R$ (k)	$\varepsilon_{t0}(\sigma)$ (m · m^{-1})	$Z(\sigma)$ (h^{-1})
ASTM A36	38,890	$3.258 \times 10^{-17\sigma 1.75}$	$2.365 \times 10^{-20\sigma 4.7}$ if $\sigma \leq 103.4 \times 106$
			$1.23 \times 10^{16} \exp(4.35 \times 10^{-8\sigma})$ if $103.4 \times 10^6 \leq \sigma \leq 310 \times 10^6$
ASTM A421	30,560	$8.845 \times 10^{-9\sigma 0.67}$	$1.952 \times 10^{-10\sigma 3}$ if $\sigma \leq 172.4 \times 10^6$
			$8.21 \times 10^{13} \exp(1.45 \times 10^{-8\sigma})$ if $172.4 \times 10^6 \leq \sigma \leq 690 \times 10^6$

σ is measured in Pa

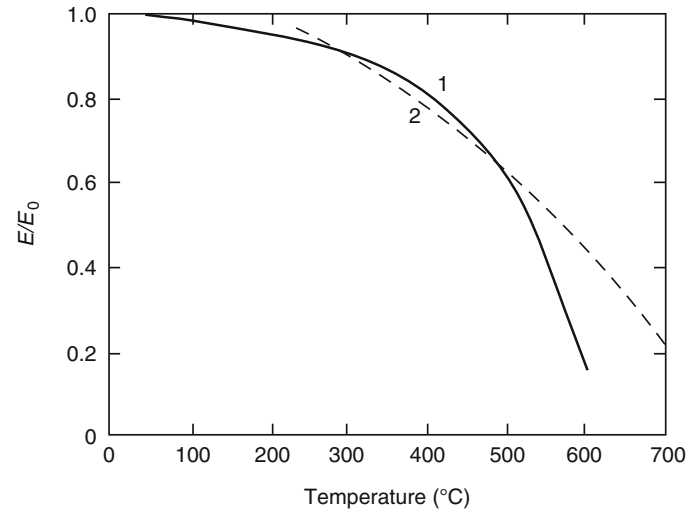

Fig. 9.11 The effect of temperature on the modulus of elasticity of (1) structural steels and (2) steel reinforcing bars [49]

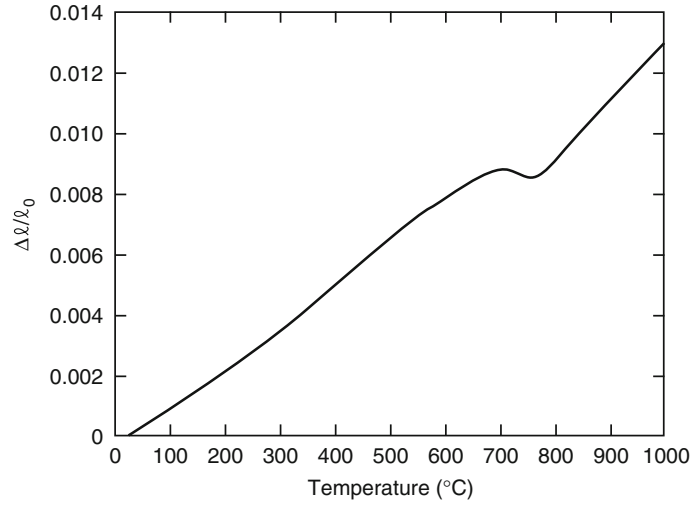

Fig. 9.12 Dilatometric curve for steel

Table 9.2 Critical temperature for various types of steel

Steel	Standard/reference	Temperature (°C)
Structural steel	ASTM	538
Reinforcing steel	ASTM	593
Prestressing steel	ASTM	426
Light-gauge steel	EC 3 [51]	350
	Gerlich et al. [55]	400

2003 [57]) are mainly based on experimental data on mild steel and do not account for specific property variations in new types of alloy steels.

Recent research by Wang et al. [58] clearly show that high strength (Q460) steel exhibits slower loss of strength and modulus throughout 20–800 °C temperature range as compared to mild steel. This is mainly due to the presence of chromium and niobium, which improves fire resistance properties of steel.

Furthermore, tests by Kodur et al. [59] have shown that type of heat treatment has significant influence on strength properties of steel e.g. annealing and normalizing produces normal strength steel, whereas quenching and tempering produces high strength steel. High strength steel, produced using quenching and tempering process, and that is used in bolts (A490 bolts) possesses slightly lower thermal conductivity than that of conventional mild steel.

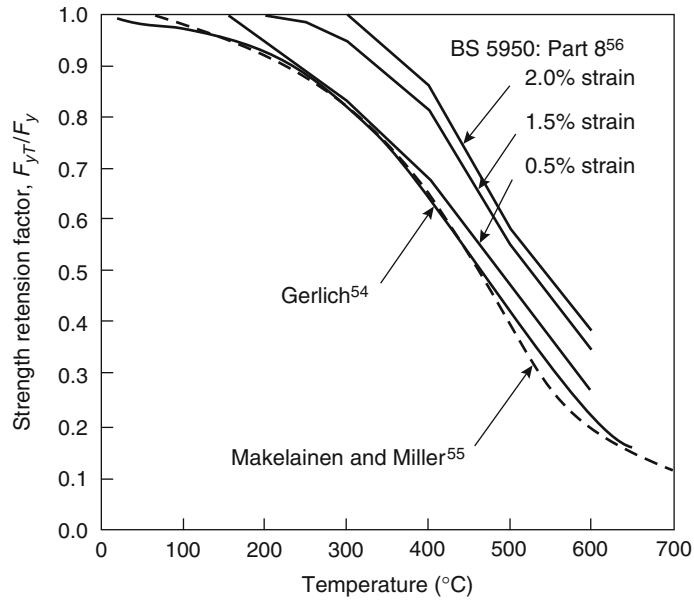

Fig. 9.13 Reduction of the yield strength of cold-formed light-gauge steel at elevated temperatures [57–61]

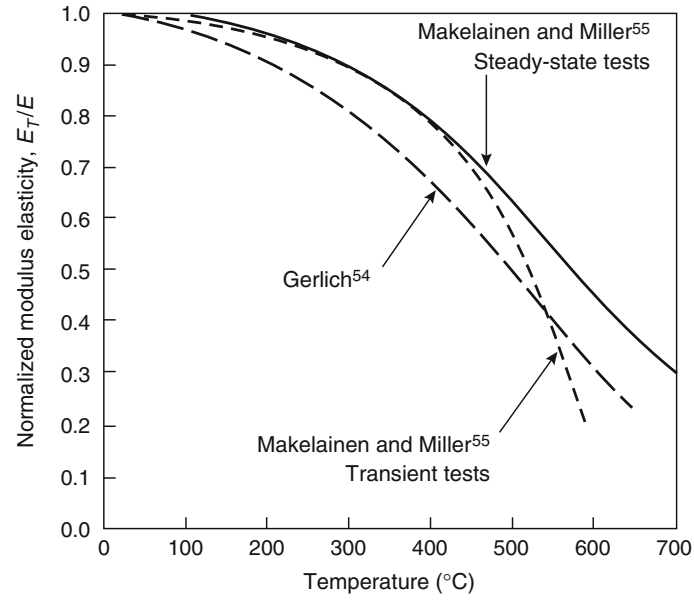

Fig. 9.14 Modulus of elasticity of cold-formed light-gauge steel at elevated temperatures [57–61]

The properties of cold-formed light-gauge steel are slightly different from those of hot-rolled structural steel. Gerlich [60] and Makelainen and Miller [61], based on steady-state and transient tests on cold-formed steel tension coupons (cut from studs) and galvanized sheets, proposed relationships for yield strength and modulus of elasticity. Figure 9.13 shows the variation of yield strength of light-gauge steel at elevated temperatures, corresponding to 0.5 %, 1.5 %, and 2 % strains based on the proposed relationships and on the relationship in BS 5950 [57]. The BS 5950 curves represent a conservative 95 % confidence limit (i.e., a 5 % chance that strength would fall below the curve), whereas the other two curves are representative of mean test data. Figure 9.14 shows the variation of modulus of elasticity of light-gauge steel at elevated

temperatures. The modulus E_T represents the tangent modulus at low stress levels (or initial tangent modulus), because steel stress-strain relationships become increasingly nonlinear at elevated temperatures. The effect of zinc coating on the mechanical properties of steel is of little significance.

The light-gauge steel has somewhat lower thermal expansion when compared to similar expressions for other steels [61]. The other thermal properties of steel, such as specific heat and thermal conductivity, are of little importance for the thermal modeling of light-gauge steel because steel framing plays a minor role in the heat transfer mechanism. A review of some of these properties is presented in a review paper [62].

The critical temperature of light-gauge steel is much lower than for other types of steels. Although Eurocode 3 limits this to a conservative value of 350 °C, in other cases a critical temperature of 400 °C is used (see Table 9.2).

Concrete

Concrete is a Group L/I material. The word *concrete* covers a large number of different materials, with the single common feature that they are formed by the hydration of cement. Because the hydrated cement paste amounts to only 24–43 volume percent of the materials present, the properties of concrete may vary widely with the aggregates used.

Traditionally, the compressive strength of concrete used to be around 20–50 MPa, which is referred to as normal-strength concrete (NSC). In recent years, concrete with a compressive strength in the range 50–100 MPa has become widely used and is referred to as high-strength concrete (HSC). Depending on the density, concretes are usually subdivided into two major groups: (1) normal-weight concretes with densities in the 2150- to 2450-kg·m^{-3} range and (2) lightweight concretes with densities between 1350 and 1850 kg·m^{-3}. Fire safety practitioners again subdivide the normal-weight concretes into silicate (siliceous) and carbonate aggregate concrete, according to the composition of the principal aggregate. Also, a small amount of discontinuous fibers (steel or polypropylene fibers) is often added to the concrete mix to achieve superior performance; this concrete is referred to as fiber-reinforced concrete (FRC). In this section, the properties of concrete are discussed under three groups: namely, NSC, FRC, and HSC.

Normal-Strength Concrete

A great deal of information is available in the literature on the mechanical properties of various types of normal-strength concrete. This information is summarized in reports by Bennetts [44] and Schneider [45], the ACI guide [43], the ASCE fire protection manual [29], and in Harmathy's book [2]. Figure 9.15 shows the stress-strain curves for a lightweight concrete with expanded shale aggregate at room temperature (24 °C) and a few elevated temperature levels [63]. The shape of the curves may depend on the time of holding the test specimen at the target temperature level before the compression test.

The modulus of elasticity (E) of various concretes at room temperature may fall within a very wide range, 5.0×10^3–35.0×10^3 MPa,

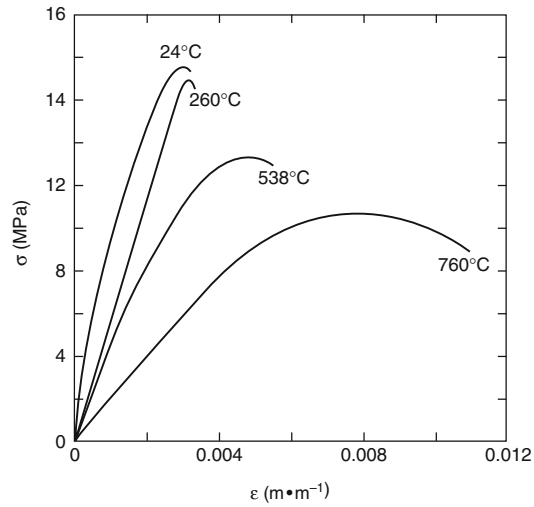

Fig. 9.15 Stress-strain curves for a lightweight masonry concrete at room and elevated temperatures [63]

dependent mainly on the water-cement ratio in the mixture, the age of concrete, the method of conditioning, and the amount and nature of the aggregates. Cruz found that the modulus of elasticity decreases rapidly with the rise of temperature, and the fractional decline does not depend significantly on the type of aggregate [64] (in Fig. 9.16, E_0 is the modulus of elasticity at room temperature). From other surveys [2, 44], it appears, however, that the modulus of elasticity of normal-weight concretes decreases faster with the rise of temperature than that of lightweight concretes.

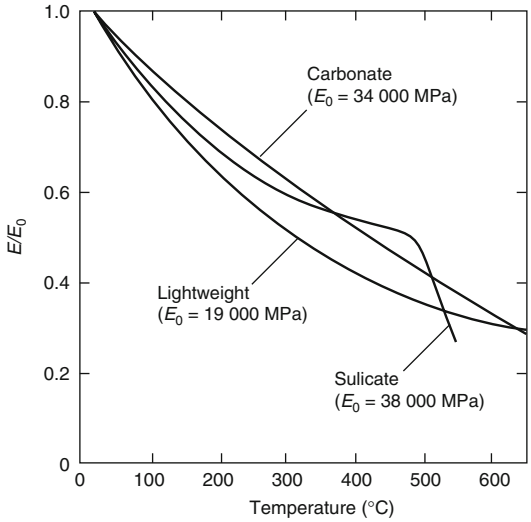

Fig. 9.16 The effect of temperature on the modulus of elasticity of concretes with various aggregates [61]

The compressive strength (σ_u) of NSC may also vary within a wide range. Compressive strength is influenced by the same factors as the modulus of elasticity. For conventionally produced normal-weight concretes, the strength at room temperature is usually between 20 and 50 MPa. For lightweight concretes, the strength is usually between 20 and 40 MPa.

Information on the variation of the compressive strength with temperature is presented in Fig. 9.17 (for a silicate aggregate concrete), Fig. 9.18 (for a carbonate aggregate concrete), and Fig. 9.19 (for two lightweight aggregate concretes, one made with the addition of natural sand) [65]. ($[\sigma_u]_0$ in the figures stands for the compressive strengths of concrete at room temperature.) In some experiments, the specimens were heated to the test temperature without load (see curves labeled "unstressed"). In others they were heated under a load amounting to 40 % of the ultimate strength (see curves labeled "stressed"). Again, in others they were heated to the target temperature without load, then cooled to room temperature and stored at 75 % relative humidity for six days, and finally tested at room temperature (see curves labeled "unstressed residual").

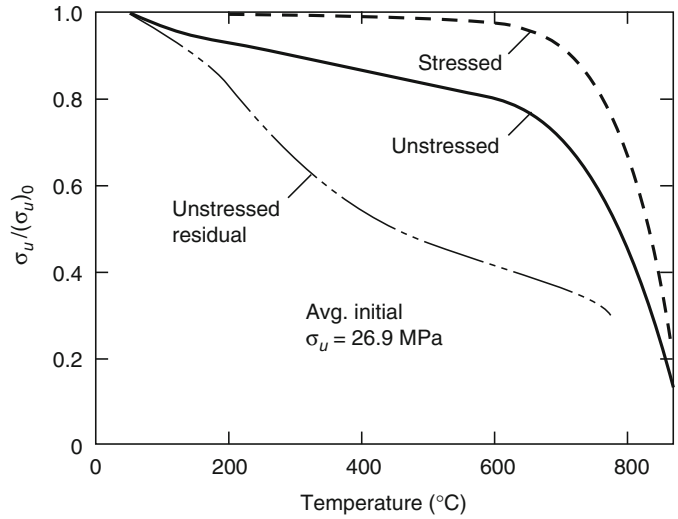

Fig. 9.17 The effect of temperature on the compressive strength of a normal-weight concrete with silicate aggregate [65]

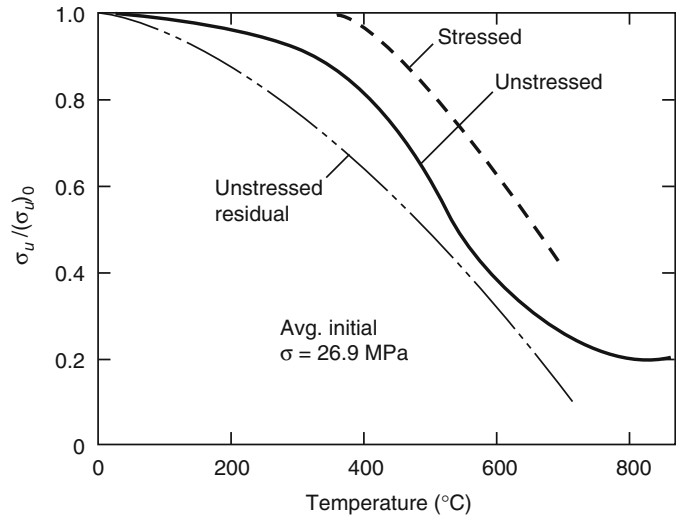

Fig. 9.18 The effect of temperature on the compressive strength of a normal-weight concrete with carbonate aggregate [65]

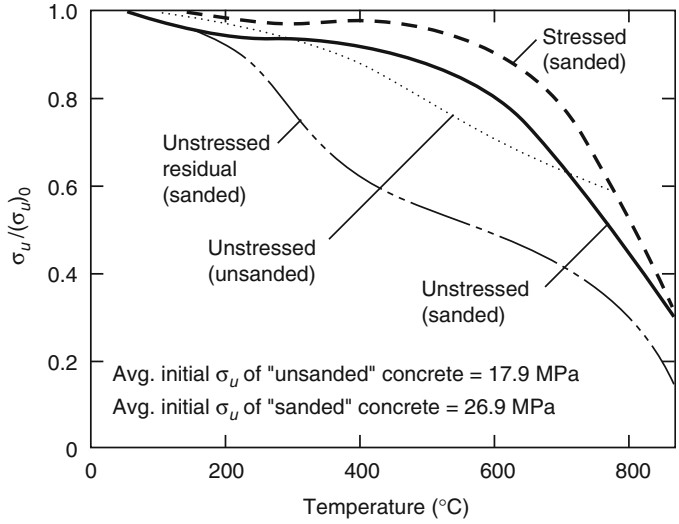

Fig 9.19 The effect of temperature on the compressive strength of two lightweight concretes (one with natural sand) [65]

Some information on the creep of concrete at elevated temperatures is available from the work of Cruz [66], MareÂchal [67], Gross [68], and Schneider et al. [69] The creep curves shown in Fig. 9.20 are those recorded by Cruz for a normal-weight concrete with carbonate aggregates.

Because the aggregates amount to 60–75 % of the volume of concrete, the dilatometric curve usually resembles that of the principal aggregate. However, some lightweight aggregates, for example, pearlite and vermiculite, are unable to resist the almost continuous shrinkage of the cement paste on heating, and therefore their dilatometric curves bear the characteristic features of the curve for the paste.

The dilatometric curves of two normal-weight concretes (with silicate and carbonate aggregates) and two lightweight concretes (with expanded shale and pumice aggregates) are shown in Fig. 9.21 [20]. These curves were obtained in the course of a comprehensive study performed on 16 concretes.

The results of dilatometric and thermogravimetric tests were combined to calculate the volumetric heat capacity (ρcp) versus temperature relation for these four concretes, as shown in

Fig. 9.22. The partial decomposition of the aggregate is responsible for a substantial drop (above 700 °C) in the density of concretes made with carbonate aggregate.

The aggregate type and moisture content have significant influence on the specific heat of concrete. The usual ranges of variation of the volume-specific heat (i.e., the product ρcp) for normal-weight and lightweight concretes are shown in Fig. 9.23. This information, derived by combining thermodynamic data with thermogravimetric observations [2, 6], has since been confirmed by differential scanning calorimetry [7]. Experimental data are also available on a few concretes and some of their constituents [2, 7].

The thermal conductivity (k) of concrete depends mainly on the nature of its aggregates. In general, concretes made with dense, crystalline aggregates show higher conductivities than those made with amorphous or porous aggregates. Among common aggregates, quartz has the highest conductivity; therefore, concretes made with siliceous aggregates are on the whole more conductive than those made with other silicate and carbonate aggregates.

Derived from theoretical considerations [6], the solid curves in Fig. 9.24 describe the variation with temperature of the thermal conductivity of four concretes. In deriving these curves, two concretes (see curves 1 and 2) were visualized to represent limiting cases among normal-weight concretes, and the other two (see curves 3 and 4), limiting cases among lightweight concretes. The points in Fig. 9.24 stand for experimental data. They reveal that the upper limiting case is probably never reached with aggregates in common use and that the thermal conductivity of lightweight concretes may be somewhat higher than predicted on theoretical considerations.

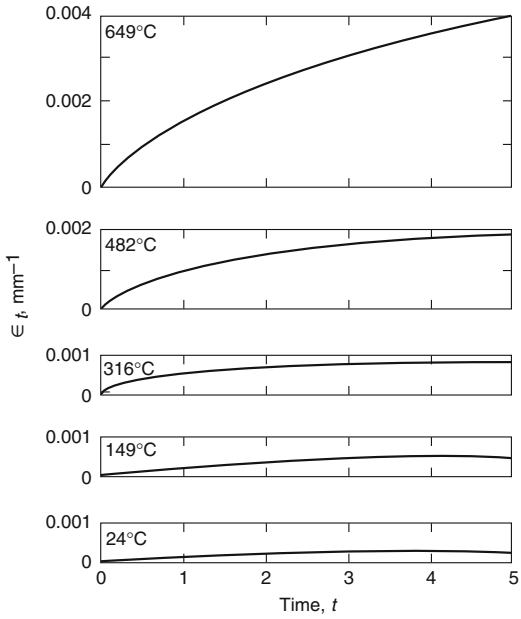

Fig. 9.20 Creep of a carbonate aggregate concrete at various temperature levels (applied stress: 12.4 MPa; compressive strength of the material at room temperature: 27.6 MPa) [66]

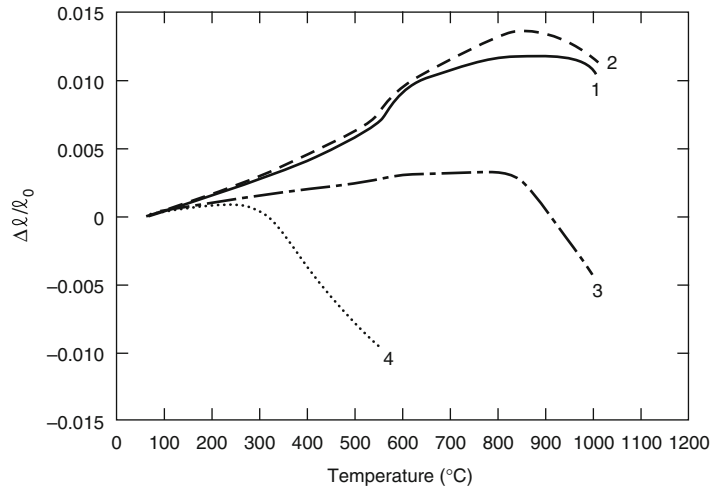

Fig. 9.21 Dilatometric curves for two normal-weight and two lightweight concretes [20]. (1) normal-weight concrete with silicate aggregate, (2) normal-weight concrete with carbonate aggregate, (3) lightweight concrete with expanded shale aggregate, (4) lightweight concrete with pumice aggregate

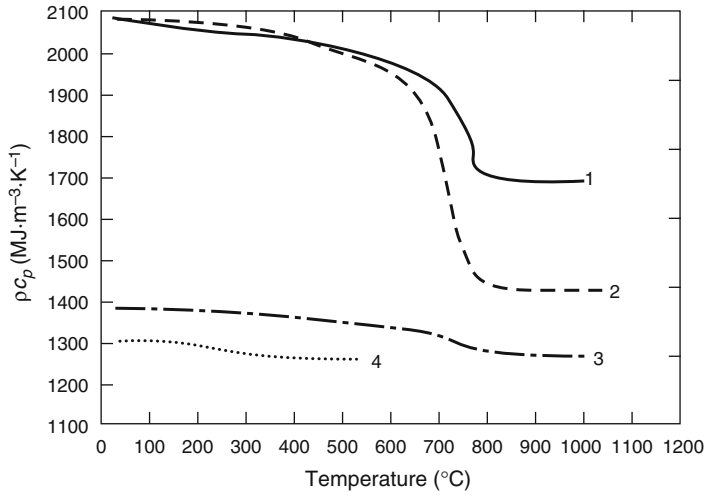

Fig. 9.22 Volumetric heat capacity of two normal-weight and two lightweight concretes [20]. (1) normal-weight concrete with silicate aggregate, (2) normal-weight concrete with carbonate aggregate, (3) lightweight concrete with expanded shale aggregate, (4) lightweight concrete with pumice aggregate

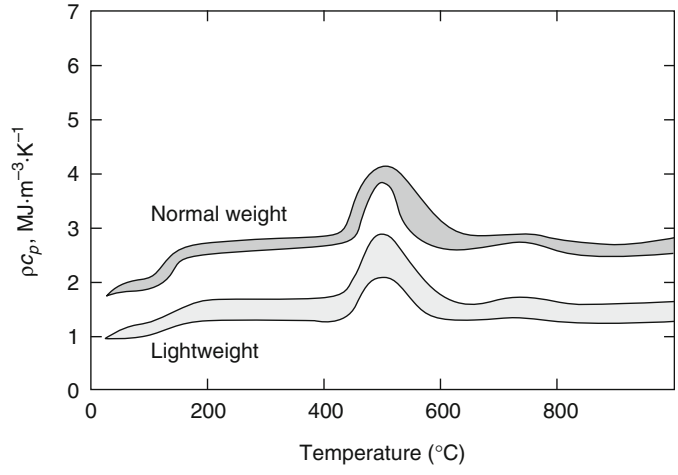

Fig. 9.23 Usual ranges of variation for the volume-specific heat of normal-weight and lightweight concretes [6]

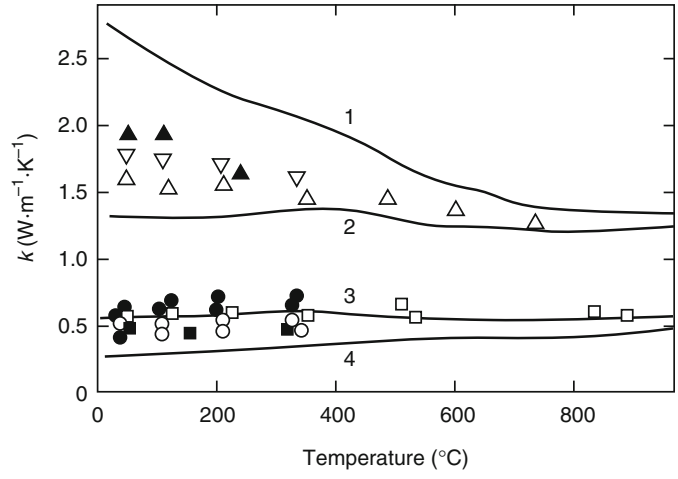

Fig. 9.24 Thermal conductivity of four "limiting" concretes and some experimental thermal conductivity data. 6,19 Symbols: ▼, ▽—various gravel concretes; ●—expanded slag concretes; ■, □—expanded shale concretes; ○—pumice concrete

Further experimental information on the thermal conductivity of some normal-weight and many lightweight concretes is available from the literature [6, 7, 20].

In reinforced concrete structures, the bond between rebars and concrete (at elevated temperatures) plays a major role in determining the fire endurance of structural members. Diederichs and Schneider investigated the variation of bond strength between deformed and plain rebars and concrete as a function of temperature [70]. They found that the bond strength reduction follows the same pattern as compressive strength for deformed and rusted plain bars. However, higher reduction in bond strength was observed for new plain bars. They also found that the bond strength at elevated temperature increases with decreasing coefficient of thermal expansion of concrete, which is significantly influenced by the type of aggregate. Diederichs and Schneider also concluded that the water-cement ratio and the bar diameter have a minor effect on the bond strength between steel and concrete [70]. Figure 9.25 illustrates the variation of bond strength as a function of temperature for reinforced and prestressed concrete.

Fiber-Reinforced Concrete

Steel and polypropylene discontinuous fibers are the two most common fibers used in the concrete mix to improve structural properties of concrete. Studies have shown that polypropylene fibers in a concrete mix are quite effective in minimizing spalling in concrete under fire conditions [71, 72]. The polypropylene fibers melt at a relatively low temperature of about 170 °C and create channels for the steam pressure in concrete to escape. This prevents the small explosions that cause the spalling of the concrete. Based on these studies, the amount of polypropylene fibers needed to minimize spalling is about 0.1–0.25 % (by volume). The polypropylene fibers were found to be most effective for HSC made with normal-weight aggregate.

The addition of fibers improves certain mechanical properties, such as tensile strength, ductility, and ultimate strain, at room temperature. However, there is very little information on the high-temperature properties of this type of concrete [73].

Steel fiber–reinforced concrete (SFRC) exhibits, at elevated temperatures, mechanical properties that are more beneficial to fire resistance than those of plain concrete. There is some information available on SFRC's material properties at elevated temperatures. The effect of temperature on the compressive strength for two types of SFRC is shown in Fig. 9.26. The strength of both types of SFRC exceeds the initial strength of the concretes up to about 400 °C. This is in contrast to the strength of plain concrete, which decreases slightly with temperatures up to 400 °C. Above approximately

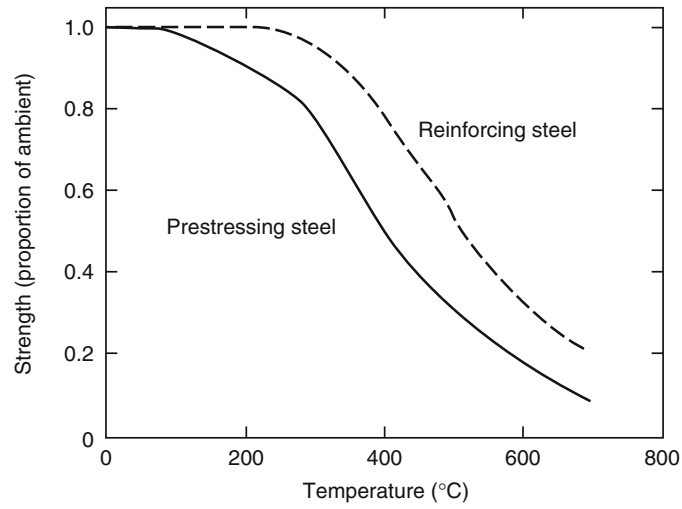

Fig. 9.25 Variation of bond strength as a function of temperature for reinforced and prestressed concrete [70]

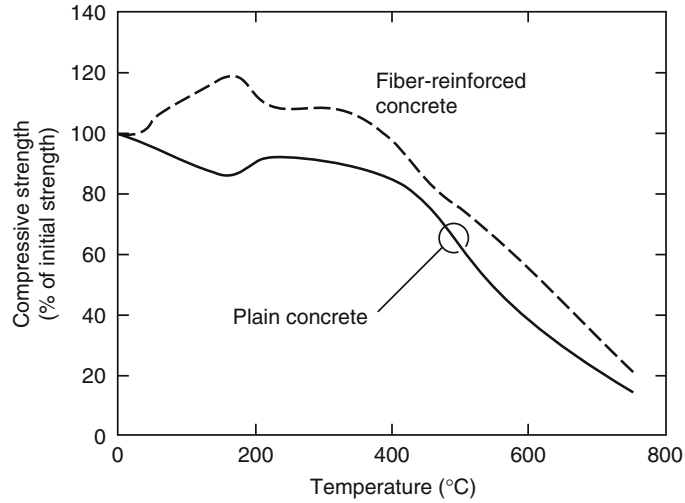

Fig. 9.26 Effect of temperature on compressive strength of steel fiber–reinforced concrete

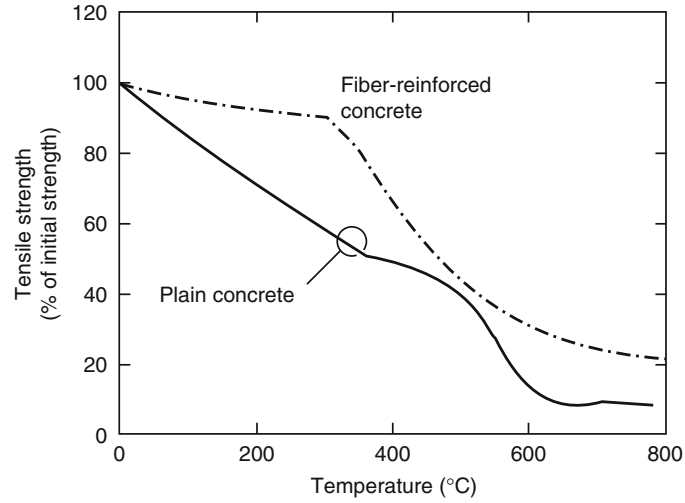

Fig. 9.27 Effect of temperature on tensile strength of steel fiber–reinforced concrete

400 °C, the strength of SFRC decreases at an accelerated rate [74].

The effect of temperature on the tensile strength of steel fiber–reinforced carbonate concretes is compared to that of plain concrete in Fig. 9.27 [75]. The strength of SFRC decreases at a lower rate than that of plain concrete throughout the temperature range, with the strength being significantly higher than that of plain concrete up to about 350 °C. The increased tensile strength delays the propagation of cracks in fiber-reinforced concrete structural members and is highly beneficial when the member is subjected to bending stresses.

The type of aggregate has a significant influence on the tensile strength of steel fiber–reinforced concrete. The decrease in tensile strength for carbonate aggregate concrete is higher than that for siliceous aggregate concrete [75].

The thermal properties of SFRC, at elevated temperatures, are similar to those of plain concrete. Kodur and Lie [27, 73] have carried out detailed experimental studies and developed dilatometric and thermogravimetric curves for various types of SFRC. Based on these studies, they have also developed expressions for thermal and mechanical properties of steel fiber–reinforced concrete in the temperature range 0–1000 °C [18, 76].

High-Strength Concrete

The strength of concrete has significant influence on the properties of HSC. The material properties of HSC vary differently with temperature than those of NSC. This variation is more pronounced for mechanical properties, which are affected by these factors: compressive strength, moisture content, density, heating rate, percentage of silica fume, and porosity [77]. The available information on the mechanical properties of HSC at elevated temperatures is presented in a review report by Phan [30].

The loss in compressive strength with temperature is higher for HSC than that for NSC up to about 450 °C. Figure 9.28 shows the comparison of strengths for NSC and HSC types, together with CEB and European design curves for NSC. The difference between compressive strength versus temperature relationships of normal-weight and lightweight aggregate concrete is not significant. However, HSC mixture with silica fume have higher compressive strength loss with increasing temperature than HSC mixture without silica fume. Based on a series of high-temperature material property tests, Kodur et al. have proposed a set of stress-strain relationships for HSC as a function of temperature [78, 79]. The variation, with temperature, of modulus of elasticity and tensile strength of HSC is similar to that of NSC.

Kodur and Sultan have presented detailed experimental data on the thermal properties of HSC (for both plain and steel fiber–reinforced concrete types) [80]. The type of aggregate has significant influence on the thermal properties of HSC at elevated temperatures. Figure 9.29 shows the thermal conductivity and specific heat of HSC, with siliceous and carbonate aggregates, as a function of temperature. Based on the test data, Kodur and Sultan have proposed relationships for thermal conductivity, specific heat, thermal expansion, and mass loss of HSC as a function of temperature [81].

The variation of thermal expansion with concrete temperature for siliceous and carbonate aggregate HSC is similar to that of NSC, with the aggregate having a strong influence. Overall, the thermal properties of HSC, at elevated temperatures, are similar to those of NSC [82].

HSC, due to low porosity, is more susceptible to spalling than NSC, and explosive spalling may occur when HSC is exposed to severe fire conditions. Hence, one of the major concerns for the use of HSC is regarding its behavior in fire, in particular, the occurrence of spalling at elevated temperatures. For predicting spalling performance, knowledge of the variation of porosity with temperature is essential. Figure 9.30 shows the variation of porosity with temperature for NSC and HSC. The data in this figure are taken from the measurements

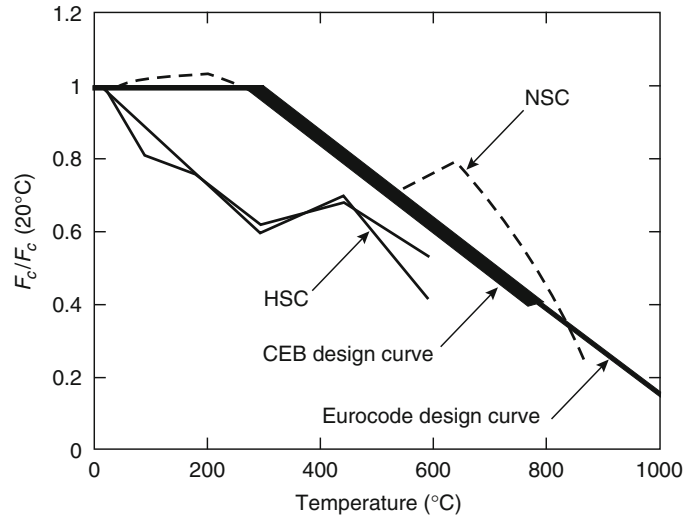

Fig. 9.28 Comparison of design compressive strength and results of unstressed tests of lightweight aggregate concrete [30]

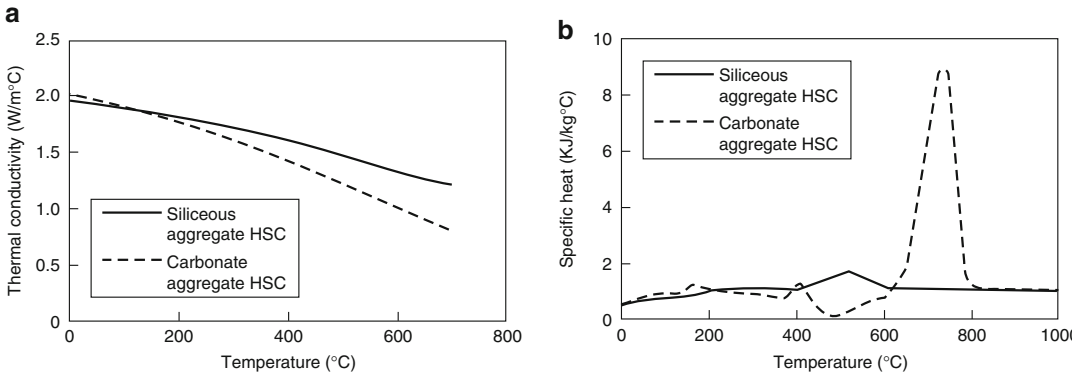

Fig. 9.29 Thermal conductivity and specific heat capacity of HSC as a function of temperature: [80] (**a**) thermal conductivity of high-strength concrete and (**b**) specific heat of high-strength concrete

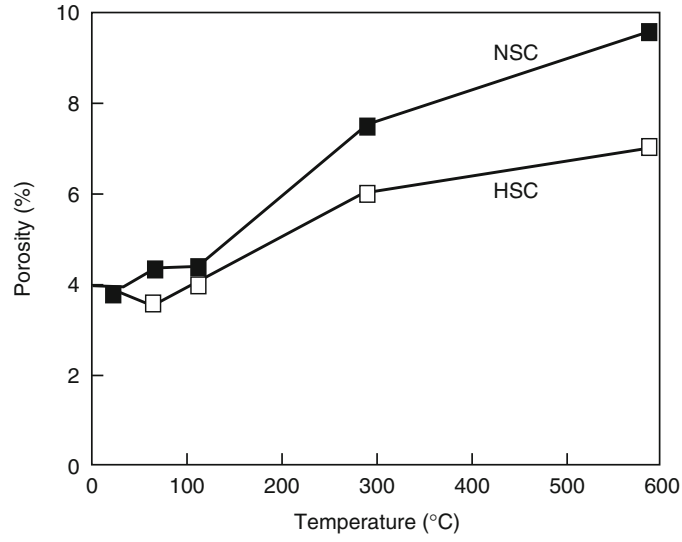

Fig. 9.30 Porosity of HSC and NSC as a function of temperature [36]

of porosity after exposure to different temperatures [36].

The spalling in HSC can be minimized by creating pores through which water vapor can be relieved before vapor pressure reaches critical values. This is usually done by adding polypropylene fibers to the HSC [71, 72, 83]. Also, Kodur et al. have reported that spalling in HSC columns can be minimized to a significant extent by providing bent ties as lateral confinement [77, 84]. Figure 9.31 illustrates conventional and improved tie configuration for minimizing spalling in HSC columns [84].

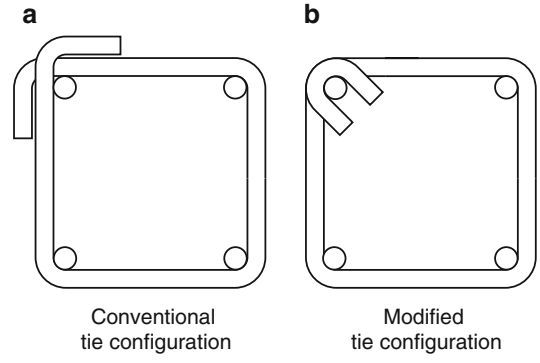

Fig. 9.31 Tie configuration for achieving higher fire resistance in concrete structures [79]

Brick

Building brick belongs in the L/I group of materials. The density (ρ) of bricks ranges from 1660 to 2270 kg·m^{-3}, depending on the raw materials used in the manufacture, and on the molding and firing technique. The true density of the material (ρt) is somewhere between 2600 and 2800 kg·m^{-3}.

The modulus of elasticity of brick (E) is usually between 10×10^3 and 20×10^3 MPa. Its compressive strength (σ_u) varies in a very wide range, from 9 to 110 MPa—50 MPa may be regarded as average [85]. This value is an order of magnitude greater than the stresses allowed in the design of grouted brickwork. Because brick is rarely considered for important load-bearing roles in buildings, there has been little interest in the mechanical properties of bricks at elevated temperatures.

At room temperature, the coefficient of thermal expansion (α) for clay bricks is about 5.5×10^{-6} m·m^{-1} K^{-1}. The dilatometric and thermogravimetric curves for a clay brick of 2180 kg·m^{-3} density are shown in Fig. 9.32 [7]. The variation with temperature of the specific heat and the thermal conductivity of this brick is shown in Figs 9.33 and 9.34, respectively [7].

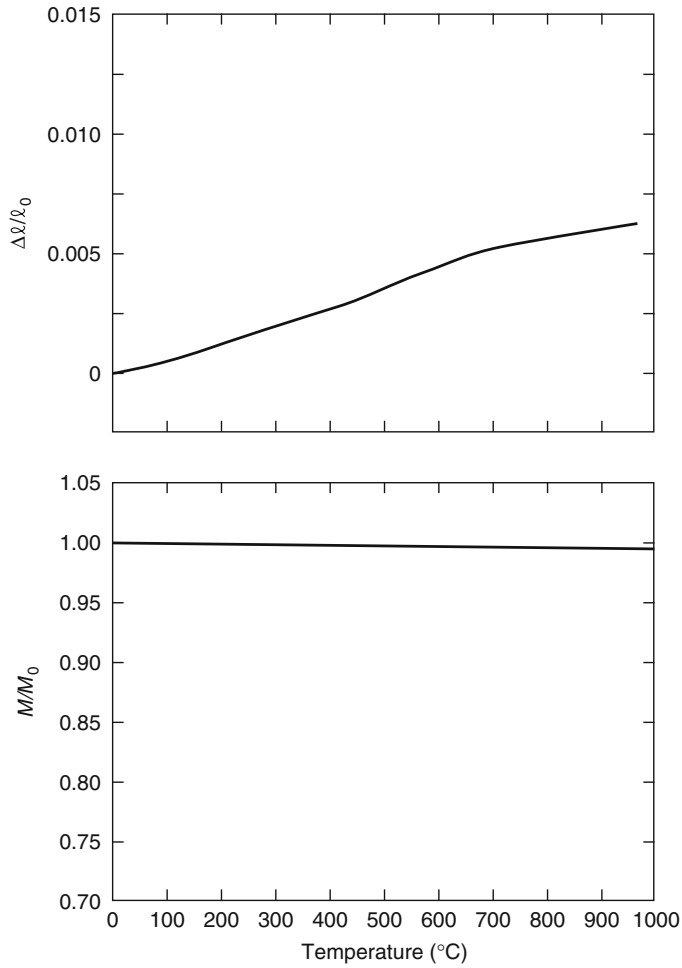

Fig. 9.32 Dilatometric and thermogravimetric curves for a clay brick [7]

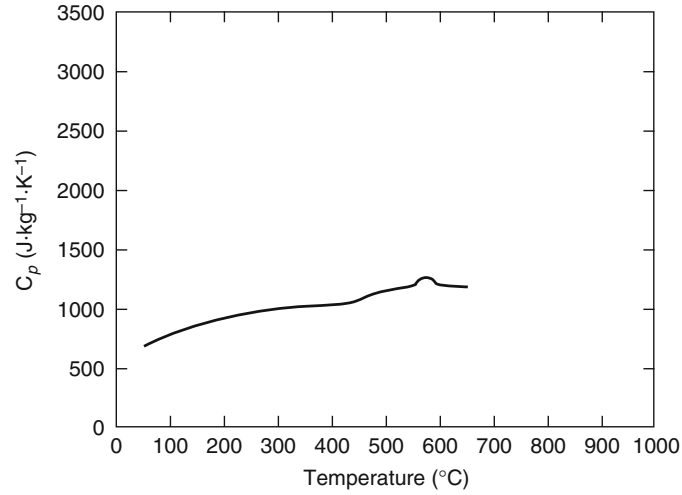

Fig. 9.33 Apparent specific heat of a clay brick [7]

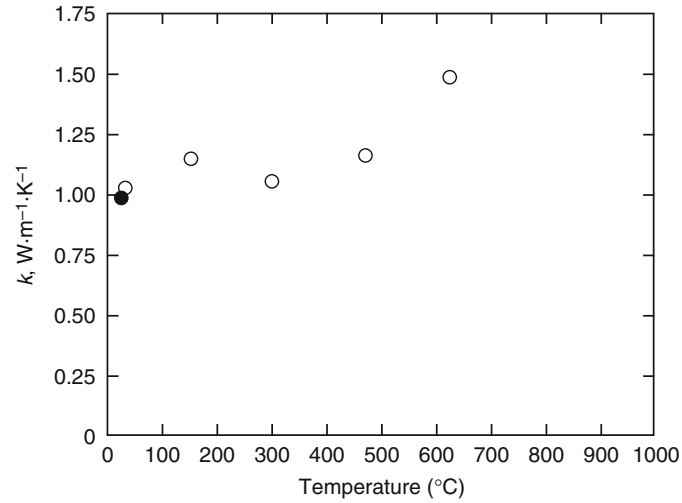

Fig. 9.34 Thermal conductivity of a clay brick. Symbols: ○—heating cycle, ●—after cooling [7]

Wood

Wood is a Group L/I/F or I/F material. As structural members, wood is widely used in residential and low-rise constructions. Although about 180 wood species are commercially grown in the United States, only about 25 species have been assigned working stresses. The two groups most extensively used as structural lumber are the Douglas firs and the southern pines.

The oven-dry density (ρ) of commercially important woods ranges from 300 kg·m^{-3} (white cedar) to 700 kg·m^{-3} (hickory, black locust). The density of Douglas firs varies from 430 to 480 kg·m^{-3} and that of southern pines from 510 to 580 kg·m^{-3}. The true density of the solid material that forms the walls of wood cells (αt) is about 1500 kg·m^{-3} for all kinds of wood. The density of wood decreases with temperature; the density ratio (ratio of density at elevated temperature to that at room temperature) drops to about 0.9 at 200 °C and then declines sharply to about 0.2 at about 350 °C [40].

Wood is an orthotropic material, so the strength and stiffness in longitudinal and transverse directions are influenced by grain orientation. The mechanical properties of wood are

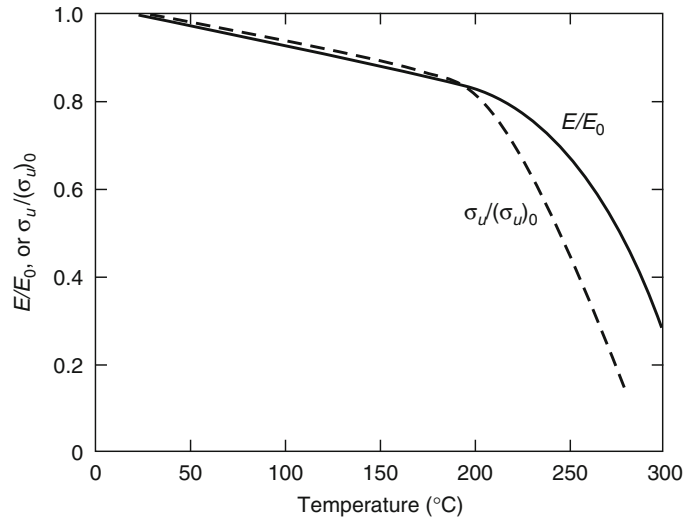

Fig. 9.35 The effect of temperature on the modulus of elasticity and compressive strength of wood [87–89]

affected by temperature and are influenced by moisture content, rate of charring, and grain orientation. The modulus of elasticity (E) of air-dry, clear wood along the grain varies from 5.5×10^3 to 15.0×10^3 MPa, and its crushing strength (σ_u) varies from 13 to 70 MPa. These properties are related and roughly proportional to the density, regardless of the species [86].

Figure 9.35 shows the variation of the modulus of elasticity and compressive strength of oven-dry, clear wood with temperature [87–89]. (E_0 and $[\sigma_u]_0$ in the figure are modulus of elasticity and compressive strength at room temperature, respectively.) The modulus of elasticity decreases slowly with temperature up to about 200 °C, when it reaches about 80 %, and then the decline is more rapid. The compressive strength also drops linearly to about 80 % at about 200 °C, and then the drop is more rapid—to about 20 % around 280 °C.

The tensile strength exhibits behavior similar to that of compressive strength, but the decline in tensile strength with temperature is less rapid. The moisture content plays a significant role in determining the strength and stiffness, with increased moisture content leading to higher reduction. There is very little information on stress-strain relationships for wood. The formulas for reduced stiffness and design strength can be found in Eurocode 5 [90] (Part 1.2).

The coefficient of linear thermal expansion (β) ranges from 3.2×10^{-6} to 4.6×10^{-6} $m \cdot m^{-1} \cdot K^{-1}$ along the grain and from 21.6×10^{-6} to 39.4×10^{-6} $m \cdot m^{-1} \cdot K^{-1}$ across the grain [91]. Wood shrinks at temperatures above 100 °C, because of the reduction in moisture content. Lie [29] reported that the amount of shrinkage can be estimated as 8 % in the radial direction, 12 % in the tangential direction, and an average of 0.1–0.2 % in the longitudinal direction. The dilatometric and thermogravimetric curves of a pine with a 400 $kg \cdot m^{-3}$ oven-dry density are shown in Fig. 9.36 [7].

The thermal conductivity (k) across the grain of this pine was measured as 0.86–1.07 $W \cdot m^{-1} \cdot K^{-1}$ between room temperature and 140 °C [14]. The thermal conductivity increases initially up to a temperature range of 150–200 °C, then decreases linearly up to 350 °C, and finally increases again beyond 350 °C.

Figure 9.37 shows the apparent specific heat for the same pine, as a function of temperature [7]. The accuracy of the curve (developed by differential scanning calorimeter [DSC]) is somewhat questionable. However, it provides useful information on the nature of decomposition reactions that take place between 150 and 370 °C.

Charring is one of the main high-temperature properties associated with wood and should be considered in predicting performance under fire

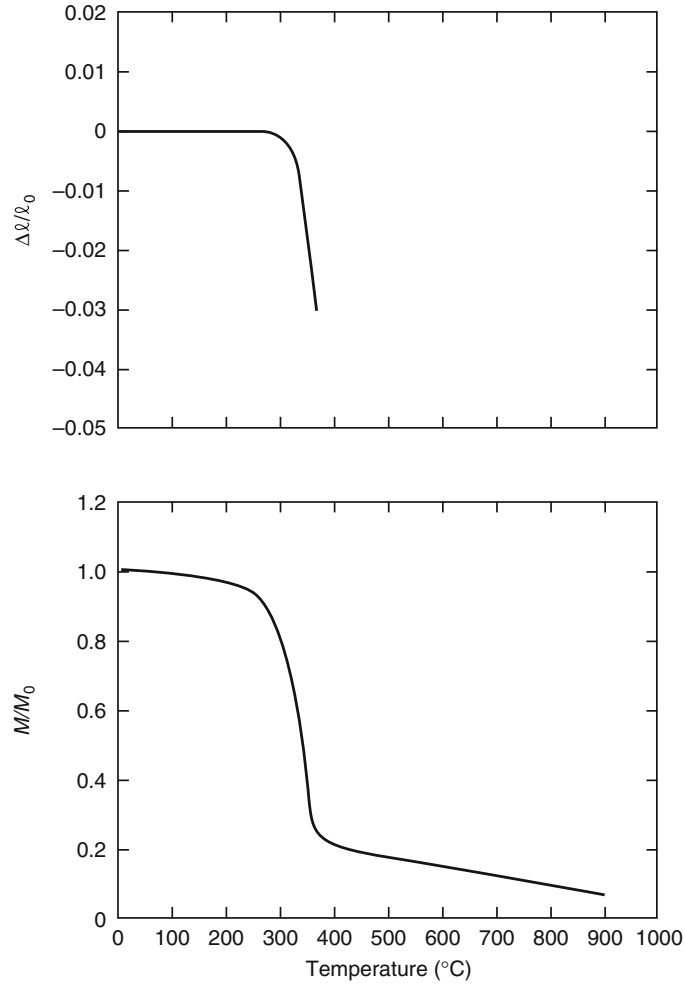

Fig. 9.36 Dilatometric and thermogravimetric curves for a pine of 400 kg·m^{-3} density [7]

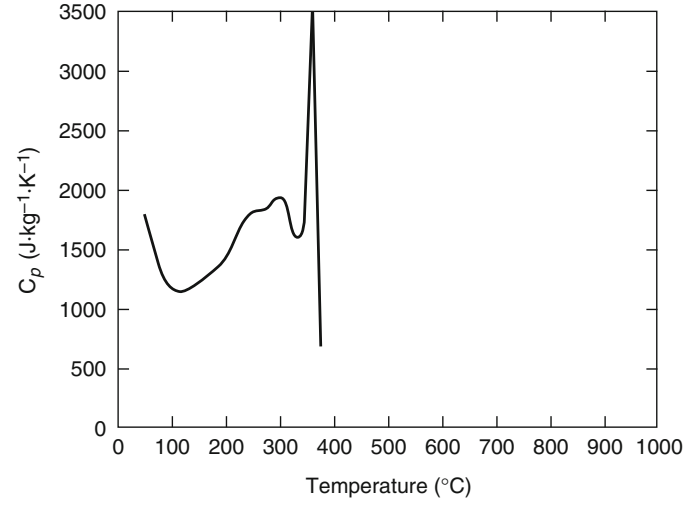

Fig. 9.37 Apparent specific heat for a pine of 400 °C density [7]

conditions. The rate of charring is influenced by the radiant heat flux or, alternatively, the fire severity. Generally, a constant transverse-to-grain char rate of 0.6 mm/min can be used for woods subjected to standard fire exposure [29]. The charring rate parallel to the grain of wood is approximately twice the rate when it is transverse to the grain. These charring rates should be used only when attempting to model the performance of wood sections in the fire resistance furnace.

Charring is influenced by a number of parameters, the most important ones being density, moisture content, and contraction of wood. It is reasonable to modify the 0.6 mm/min to approximately 0.4 mm/min for moist dense wood or to 0.8 mm/min for dry and light wood. The fire retardants often used to reduce flame spread in wood may only slightly increase the time until ignition of wood.

Specific charring rates for different types of wood can be found in "Structural Fire Protection" [29] and Bénichou and Sultan [40]. Eurocode [90] gives an expression for charring depth in a wood member exposed to standard fire. The dependence of charring rate on the radiant heat flux is discussed in *Wood Handbook* [87].

In recent years different types of engineered wood is widely used in residential construction. These engineered wood products (ex: joists and studs) capitalize on the strength of wood and the efficiency of the sectional shapes (ex: I-shaped joists) to enhance load bearing capacity at ambient conditions, while at the same time reducing the mass and cost of the structural member. However, there is very limited data on high temperature thermo-mechanical properties of engineered lumber and fire resistance of engineered joists and studs. Limited research has clearly shown that fire resistance of engineered joists to be significantly lower than that of conventional wood joists [92]. This was mainly attributed to poor thermal, mechanical and charring properties of engineered lumber as compared to conventional wood products. Typically, room temperature thermal conductivity and modulus of elasticity of engineered lumber is higher than other types of wood due to the presence of compressed plies [92]. Comparison of charring rates indicate that engineered lumber has higher rate of charring rate as compared to conventional wood [92].

Fiber-Reinforced Polymers

In recent years, there has been a growing interest in the use of fiber-reinforced polymers (FRPs) in civil engineering applications due to the advantages, such as high strength and durability (resistance to corrosion), that FRP offers over traditional materials. FRP composites consist of two key elements, namely the fibers (glass, carbon, or aramid) and a thermosetting polymer matrix such as epoxy, vinyl ester, phenolic, or polyester resin. The commonly used types of FRP composite materials are glass fiber–reinforced plastic (GFRP), carbon fiber–reinforced plastic (CFRP), and aramid fiber–reinforced plastic (AFRP) composites. FRPs are similar to wood in that they will burn when exposed to fire and can be classified as an L/I/F type material.

FRP is used as an internal reinforcement (reinforcing bars as an alternative to traditional steel reinforcement) and as external reinforcement in forms, such as wrapping and sheeting for the rehabilitation and strengthening of concrete members. One of the main impediments to using FRPs in buildings is the lack of knowledge about the fire resistance of FRP [93, 94].

There are some major differences associated with FRP as a material. The properties depend on the type and composition of FRP, and the availability of various types of FRP makes it difficult to establish the properties at elevated temperatures. The material properties are controlled by the fibers in the longitudinal direction and by the matrix in the transverse direction. In addition to thermal and mechanical properties, factors such as burning, charring, evolution of smoke, and toxicity in fire also play a significant role in determining the fire performance. A summary of typical mechanical properties for various types of FRPs, in comparison to other commonly used construction materials, at room temperature, is presented in Table 9.3.

Table 9.3 Properties of various FRP composites and other materials

Material	Modulus of elasticity E_1 (MPa)	Modulus of elasticity E_2 (MPa)	Tensile strength σ_{t1} (MPa)	Comp. strength σ_{c1} (MPa)	Shear modulus G (MPa)	Shear strength S (MPa)	Poisson's ratio ν	Tensile strength σ_2 (MPa)	Comp. strength σ_{c2} (MPa)
GFRP (glass/epoxy)	55,000	18,000	1050	1050	9000	42	0.25	28	140
GFRP (glass/epoxy) unidirectional	42,000	12,000	700	—	5000	72	0.30	30	—
CFRP (carbon/epoxy) unidirectional	180,000	10,000	1500	—	7000	68	0.28	40	—
CFRP (graphite/epoxy)	207,000	5200	1050	700	2600	70	0.25	40	120
Boron/epoxy	207,000	21,000	1400	2800	7000	126	0.30	84	280
ARP (aramid/epoxy) unidirectional	76,000	8000	1400	—	3000	34	0.34	12	—
Mild steel	200,000	—	550	240	—	380	—	—	—
Concrete (normal strength)	31,000	—	~4	40	—	~7	0.15–0.20	—	—
Wood (Douglas fir)	9800	—	69	—	—	—	—	—	—

E_1 = modulus of elasticity in longitudinal direction
E_2 = modulus of elasticity in transverse direction

There is very little information on the material properties of FRPs at elevated temperatures [93]. The impact of high temperatures on the behavior of FRP composites is severe degradation of their properties: reduction of strength and stiffness, and increase in deformability, thermal expansion, and creep. Above 100 °C temperature, the degradation can be quite rapid as the glass transition temperature of the matrix is reached.

The glass transition temperature, which is often considered the upper use temperature, varies with the type of resin used and was found to be as low as 100 °C in some resins and as high as 220 °C in others. From the limited studies, it appears that as much as 75 % of the GFRP strength and stiffness is lost by the time the temperature reaches 250 °C [93, 95].

The stress-strain relationships, from the studies conducted by Gates [95], for a CFRP composite (IM7/5260) are shown in Fig. 9.38 for various temperatures. It can be seen that the tensile strength of IM7/5260 composite reduces to approximately 50 % at about 125 °C and to about 75 % at a temperature of 200 °C. The strain level, for a given stress, is also higher with the increase in temperature. Recently, Wang and Kodur reported high temperature strength and stiffness properties of glass and carbon FRP rebars; full details of the tests are reported in Wang and Kodur [96].

The variation of strength with temperature (ratio of strength at elevated temperature to that at room temperature) for FRP along with that of other traditional construction materials is shown in Fig. 9.2. The curve showing the strength degradation of FRP is based on the limited information reported in the literature [93, 95]. The rate of strength loss is much greater for FRP than for concrete and steel, resulting in a 50 % strength loss by about 200 °C.

The bond between FRPs and concrete (or between FRP layers or lap splices in multiply layup applications) is essential to transfer loads. This load transfer occurs through the polymer resin matrix and thus relies heavily on the mechanical properties of the polymer.

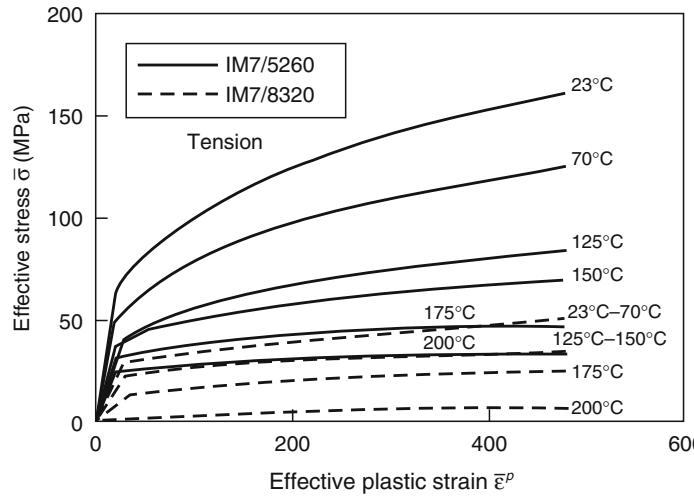

Fig. 9.38 Tensile stress-strain curves for CFRP at various temperatures [95]

Deterioration of the mechanical properties of the matrix material at temperatures above the specific polymer's glass transition temperature, T_g, have the potential to cause loss of bond at only modestly increased temperatures, resulting in loss of interaction between FRP and concrete. The glass transition temperature of commonly used polymer matrix materials is typically in the range of 65–140 °C.

No specific research has yet been reported on the bond between concrete and externally bonded FRP strengthening systems at high temperature, although limited data on the high-temperature residual performance of the FRP concrete bond has recently been presented [97].

Research on the bond properties of FRP bars for concrete reinforcement applications (internal reinforcement) at elevated temperature has been reported in the literature [98–101]. This work has indicated that dramatic decreases in bond strength can be expected, to values of about 10 % of room temperature strength, at temperatures between 100 and 200 °C (i.e., at temperatures close to or above T_g). The observed bond strength reductions have been attributed to changes in the properties of the polymer matrix at the surface of the FRP bars.

It seems clear that temperature effects on the FRP–FRP and FRP–concrete bond are critical, both in FRP internal reinforcement and in externally bonded FRP applications, and a great deal of additional research is required in this area. Thus, bond degradation at elevated temperature is a critical factor to be considered in the design of FRP-reinforced or -strengthened concrete members. This was observed in full-scale fire tests on FRP-strengthened reinforced concrete columns [102].

The critical temperature of FRP is much lower than that for steel and depends on the composition of fibers and matrix. Kodur and Baingo have assumed a critical temperature of 250 °C in modeling the behavior of FRP-reinforced concrete slabs [93]. Recently, Wang and Kodur have developed critical temperature information for glass and carbon FRP reinforcing rebars [103, 104].

They carried out a series of tensile strength tests at high temperatures on two types of commercially available FRP rebars. This included both carbon FRP and glass FRP bars of different diameters. Conventional steel rebars were also tested for comparison. The data were used to determine the variation of average failure strength and elastic modulus for each type of reinforcement with increasing temperature. Full details of experimental studies, including specimen preparation, test setup, test procedure, and observations as well as test data, are described elsewhere [96, 104].

A summary of the results of these studies are shown in Fig. 9.39. For the GFRP and CFRP bars, observed failure strengths were used, whereas for the steel bars, the 0.2 % proof stress was used. The elastic modulus was taken as the

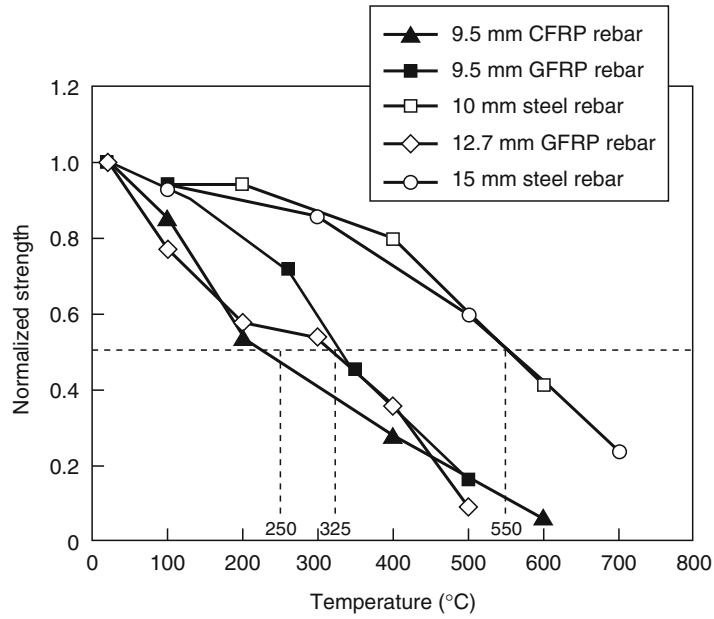

Fig. 9.39 Effect of strength degradation as a function of temperature for FRP [96]

Table 9.4 Thermal properties of various FRPs and other materials at room temperature

	Coefficient of thermal expansion (unidirectional) (β: 10^{-6} m · m^{-1}·°C)		Thermal conductivity k (W · m^{-1} ° C^{-1})	
Material	Longitudinal α_L	Transverse α_T	Longitudinal k_L	Transverse k_T
Glass/epoxy (S-glass)	6.3	19.8	3.46	0.35
Glass/epoxy (E-glass: 63 % fiber)	7.13	—	—	—
Carbon/epoxy (high modulus)	–0.9	27	48.4–60.6	0.865
Carbon/epoxy (ultra-high modulus)	–1.44	30.6	121.1–129.8	1.04
Boron/epoxy	4.5	14.4	1.73	1.04
Aramid/epoxy (Kevlar 49)	–3.6	54	1.73	0.73
Concrete	6.16		1.36–1.90	
Steel	10.8–18		15.6–46.7	
Epoxy	—	54–90	—	0.346

slope of a straight line fitted to the initial linear portion of the recorded stress-strain relationship for each specimen. The critical temperature for the FRP reinforcement was derived based on a 50 % tensile strength reduction, as is the case for steel reinforcement. This resulted in critical temperatures of about 325 °C and 250 °C for GFRP and CFRP reinforcing bars, respectively. These critical temperatures are significantly less than 593 °C, the critical temperature for steel reinforcement, thus highlighting the presumed susceptibility of FRP reinforcement to fire. Figure 9.39 also shows that the steel reinforcing bars in these tests lost about 50 % of their room-temperature yield strength at about 550 °C, a result that agrees well with published data available in the literature.

The variation of elastic moduli of FRP with temperature is different in each direction. Typical values for various types of FRP are given in Table 9.3 [93]. The three values represent the longitudinal, transverse, and shear moduli, respectively, of different unidirectional FRPs. At high temperature, the elastic moduli of FRPs decreases at a faster rate than that for concrete or steel.

Similar to mechanical properties, the thermal properties of FRP are also dependent on direction, fiber type, fiber orientation, fiber volume fraction, and laminate configuration. Table 9.4 shows thermal properties for various types of

FRP at room temperature. In the longitudinal direction, the thermal expansion of FRPs is lower than that of steel. However, in the transverse direction, it is much higher than that of steel. Some of the information available in the literature can be found in a review report by Kodur and Baingo [93]. At room temperatures, FRPs in general have low thermal conductivity, which makes them useful as insulation materials. With the exception of carbon fibers, FRPs have a low thermal conductivity.

Information on the thermal properties of FRP at elevated temperatures is very scarce, which is likely due to the fact that such information is proprietary to the composite materials' manufacturers. Also, there is not much information on evolution of smoke and toxins in FRP composites exposed to fire.

Thermal expansion of FRP reinforcement varies in longitudinal and transverse directions, and the coefficient of thermal expansion highly depends on type of fiber, resin, and volume fraction of fiber. The longitudinal coefficient of thermal expansion is dominated by properties of the fiber, while the transverse coefficient is dominated by properties of the resin. Figure 9.40

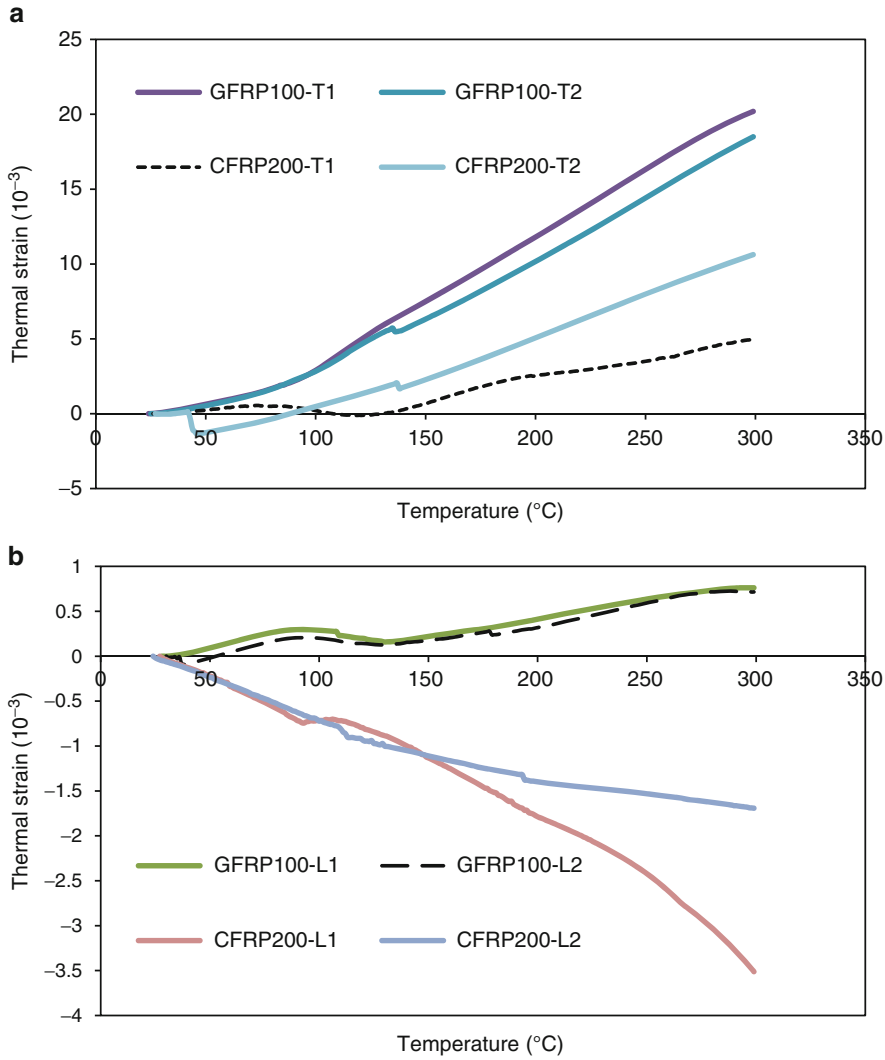

Fig. 9.40 Variation of thermal strain in GFRP and CFRP in (**a**) longitudinal and (**b**) transverse directions as a function of temperature

(a and b) shows longitudinal and transverse coefficients of thermal expansion for typical GFRP and CFRP bars. It can be noted that usually there is a change in expansion rate at around glass transition temperature (Tg), indicating FRP reinforcement experiences different coefficients of thermal expansion before and after phase change (Tg). In transverse direction, the dimension of GFRP and CFRP rebars increase with temperature, and GFRP undergoes higher thermal expansion than that of CFRP. However, in longitudinal direction, GFRP rebar slightly expands with temperature, but CFRP rebar contracts with increase in temperature. The coefficients of thermal expansion in transverse direction for GFRP and CFRP rebars can be taken to be 64.5 and 7.79×10^{-6}/°C, respectively, while the corresponding coefficients of thermal expansion in longitudinal direction are 2.48 and -7.6×10^{-6}/°C, respectively [105]

Gypsum

Gypsum (calcium sulfate dihydrate: $CaSO_4 \cdot 2H_2O$) is a Group I material. Gypsum board is produced by mixing water with plaster of paris (calcium sulfate hemihydrate: $CaSO_4 \cdot {}^1/_2H_2O$) or with Keene's cement (calcium sulfate anhydrite: $CaSO_4$). The interlocking crystals of $CaSO_4 \cdot 2H_2O$ are responsible for the hardening of the material.

Gypsum products are used extensively in the building industry in the form of boards, including wallboard, formboard, and sheathing. The core of the boards is fabricated with plaster of paris, into which weight- and set-controlling additives are mixed. Furthermore, plaster of paris, with the addition of aggregates (such as sand, pearlite, vermiculite, or wood fiber) is used in wall plaster as base coat, and Keene's cement (neat or mixed with lime putty) is used as finishing coat.

Gypsum board, based on composition and performance, is classified into various types, such as regular gypsum board, type X gypsum board, and improved type X gypsum board. A gypsum board with naturally occurring fire resistance from the gypsum in the core is defined as regular gypsum. When the core of the gypsum board is modified with special core additives or with enhanced additional properties, to improve the natural fire resistance from regular gypsum board, it is classified as type X or improved type X gypsum board. There might be significant variation in fire performance of the gypsum board based on the type and the formulation of the core, which varies from one manufacturer to another.

Gypsum is an ideal fire protection material. The water inside the gypsum plays a major role in defining its thermal properties and response to fire. On heating, it will lose the two H_2O molecules at temperatures between 125 and 200 °C. The heat of complete dehydration is 0.61×10^6 J/kg gypsum. Due to the substantial absorption of energy in the dehydration process, a gypsum layer applied to the surface of a building element is capable of markedly delaying the penetration of heat into the underlying load-bearing construction.

The thermal properties of the gypsum board vary depending on the composition of the core. The variation with temperature of the volume specific heat (ρcp) of pure gypsum has been illustrated in Harmathy [106], based on information reported in the literature [107, 108]. The thermal conductivity of gypsum products is difficult to assess, owing to large variations in their porosities and the nature of the aggregates. A typical value for plaster boards of about 700 $kg \cdot m^{-3}$ density is 0.25 $W \cdot m^{-1} \cdot K^{-1}$. Figures 9.41 and 9.42 illustrate the typical variation of the thermal conductivity and the specific heat, respectively, of the gypsum board core with temperature. The plots reflect the expressions proposed recently by Sultan [109], based on tests conducted on type X gypsum board specimens. The specific heat measurements were carried out at a heating rate of 2 °C/min. The dehydration of gypsum resulted in the two peaks that appear in the specific heat curve at temperatures around 100 °C and 650 °C. The peak values are slightly variant to those reported earlier by Harmathy [16]; this may be due to the differences in gypsum composition.

The coefficient of thermal expansion (β) of gypsum products may vary between

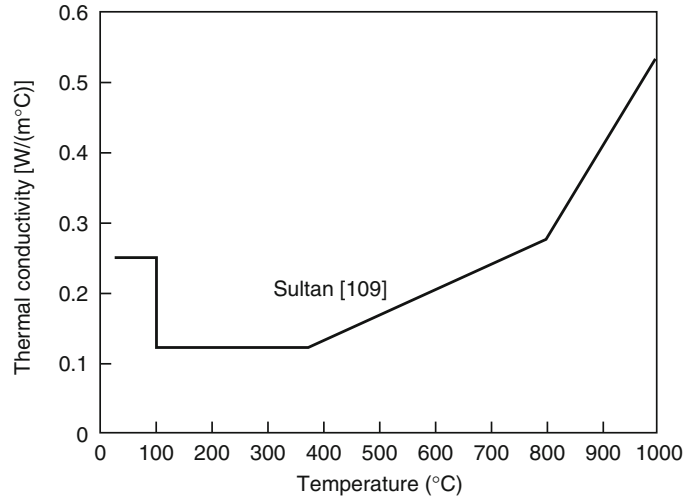

Fig. 9.41 Thermal conductivity of type X gypsum board core as a function of temperature [109]

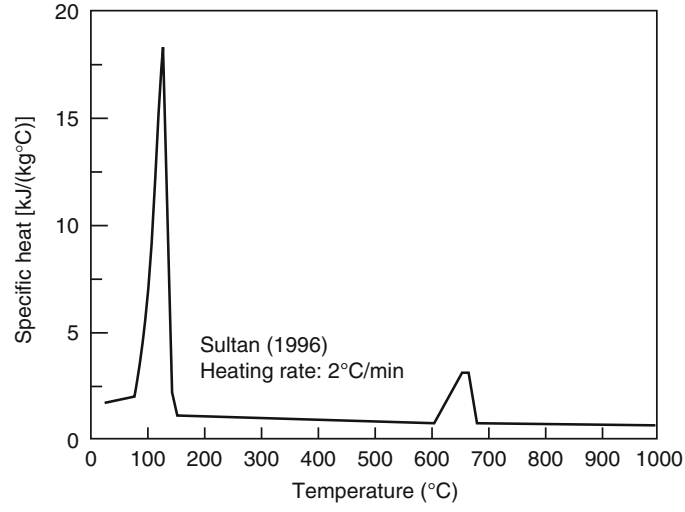

Fig. 9.42 Specific heat of type X gypsum board core as a function of temperature [109]

11.0×10^{-6} and 17×10^{-6} $m \cdot m^{-1} \cdot K^{-1}$ at room temperature, depending on the nature and amount of aggregates used. The dilatometric and thermogravimetric curves of a so-called fire-resistant gypsum board of 678 $kg \cdot m^{-3}$ density are shown in Fig. 9.43.

There is not much information about the mechanical properties of the gypsum board at elevated temperatures because these properties are difficult to obtain experimentally. The strength of gypsum board at an elevated temperature is very small and can be neglected. The Gypsum Association [110] lists typical mechanical properties, at room temperature, for some North American gypsum board products. The attachment details (screw spacing, orientation of gypsum board joints, stud spacing, etc.) may have a noticeable effect on the fire performance of the gypsum board.

Insulation

Insulation is a Group I material and is often used as a fire protection material both for heavy structural members such as columns and beams and for lightweight framing assemblies such as floors and walls. The insulation helps delay the

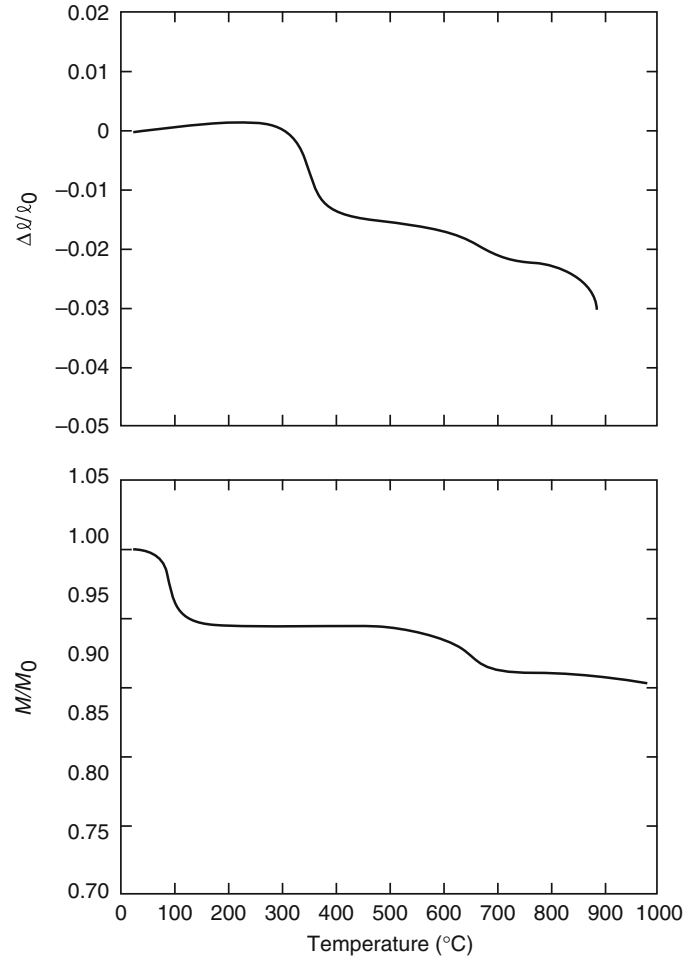

Fig. 9.43 Dilatometric and thermogravimetric curves for a gypsum board of 678 kgm^{-3} density [7]

temperature rise of structural members, thereby enhancing fire resistance. There are a number of insulation materials available in the market. Mineral wool and glass fiber are the two most widely used insulation materials in walls and floors. Other insulation materials used for fire protection include intumescent paints, spray mineral fibers, insulation boards, and compressed fiber board.

The thermal properties of insulation play an important role in determining the fire resistance. However, there is not much information available on the thermal properties of various types of insulation. Figure 9.44 shows the variation of thermal conductivity with temperature for glass and rock fiber insulation types. The differences in thermal conductivity values at higher temperatures are mainly due to variation in the chemical composition of fiber.

Full-scale fire resistance tests on walls and floors have shown that the mineral fiber insulation performs better than glass fiber insulation. This is mainly because glass fiber melts in the temperature range of 700–800 °C and cannot withstand direct fire exposure. The melting point for mineral fiber insulation is higher. The density of glass fiber is about 10 kg/m^3 and is much lower than that of rock fiber, which is about 33 kg/m^3.

The mineral wool insulation, when installed tightly between the studs, can be beneficial for the fire resistance of non-load-bearing steel stud walls because it acts as an additional fire barrier

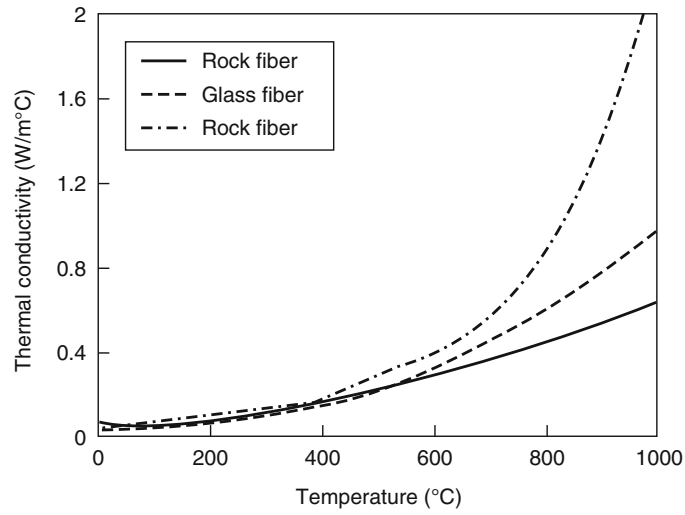

Fig. 9.44 Thermal conductivity of insulation as a function of temperature [40]

Table 9.5 Properties of some commonly used insulation materials [105]

Material	Density ρ (kg/m3)	Thermal conductivity k (W/m·K)	Specific heat c (J/kg·K)	Equilibrium moisture content %
Spray				
Sprayed mineral fibers	300	0.12	1200	1
Perlite or vermiculite plaster	350	0.12	1200	15
High-density perlite or vermiculite plaster	550	0.12	1200	15
Boards				
Fiber silicate or fiber calcium silicate	600	0.15	1200	3
Gypsum plaster	800	0.2	1700	20
Compressed fiber boards				
Mineral wool, fiber silicate	150	0.2	1200	2

after the fire-exposed gypsum board falls off [111]. On the other hand, cavity insulation slows down the flow of heat through the wall assembly and can cause an accelerated temperature rise in the fire-exposed gypsum board.

Another common form of fire insulation applied on steel structural members to achieve required fire resistance is spray applied fire resistive materials (SFRM), which work by delaying temperature rise in steel. SFRM, available under different trade names, offers several advantages over other types of fire insulation such as cost effectiveness, ease of application, and light weight, and therefore is widely used as fire proofing material for steel structures. SFRM is mainly composed of base materials such as gypsum, cementitious and mineral fiber and other additives such as vermiculite.

The thermal properties of some of the commonly used insulation systems are given in Table 9.5 [112]. It should be noted that these values are average property values and can vary depending on the manufacturer and on the proportions of different constituent materials. Also the moisture content of the insulation material has an effect on the thermal properties.

The above listed thermal properties for fire insulation are at room temperature and they can vary significantly with temperature and also with insulation composition, which can vary for different trade names (from different commercial manufactures) among the same type of insulation

(ex: SFRM). However, in practice fire resistance of insulated structural (steel) members is evaluated by considering only room temperature thermal properties of fire insulation [113]. This is mainly due to lack of reliable data on the effect of temperature on thermal properties of fire insulation. Further, there is no data on relative thermal performance of similar fire insulation products (ex: SFRM) produced from different commercial manufactures.

Figure 9.45a shows variation of thermal conductivity with temperature for three types of commercially available SFRM (A, B, and C) generated in a recent research study [114]. The thermal conductivity of three SFRM types at room temperature is in the range of 0.07 and 0.2 W/m.K. This variation of thermal conductivity among three types of SFRM well pertains to the variation in their densities and also to composition of ingredients in each type. The trends in the figure further indicate that temperature has significant effect on thermal conductivity of SFRM. This variation in thermal conductivity at higher temperatures is primarily governed by changes in moisture content and density of different SFRM types.

Insulation materials such as SFRM experience shrinkage at higher temperatures, as opposed to expansion phenomenon in materials such as steel, concrete and wood. The variation of thermal strain for three types of SFRM is plotted as a function of temperature in Fig. 9.45b [114]. This variation of thermal strain with temperature is also linked to changes in moisture content.

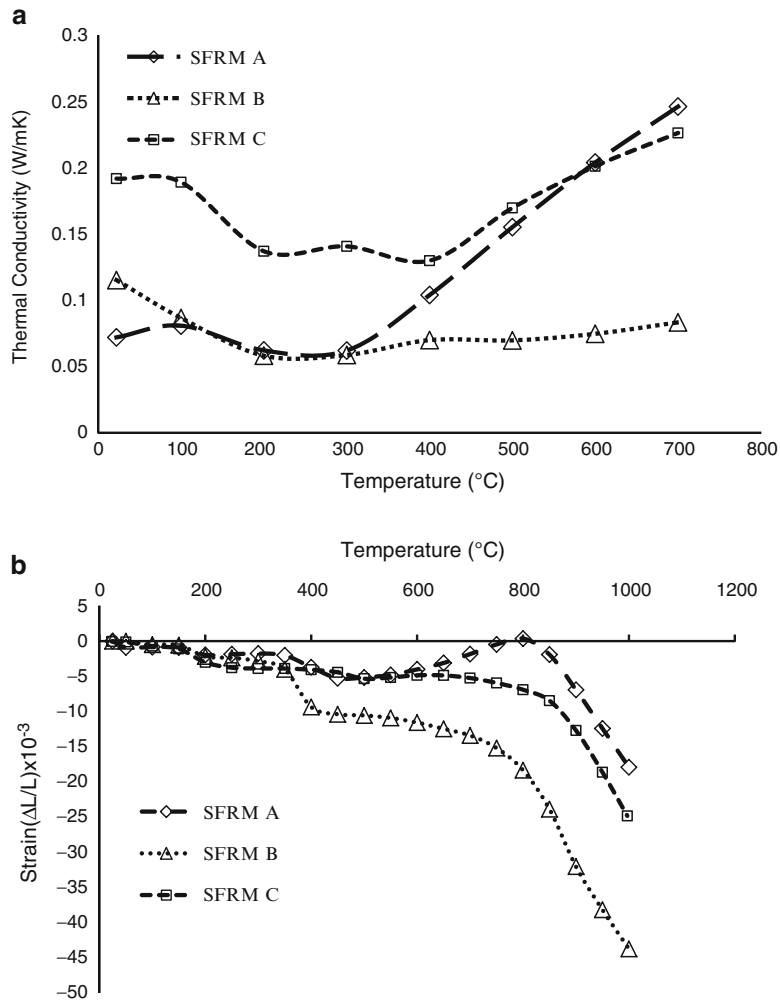

Fig. 9.45 Effect of temperature on (**a**) thermal conductivity and (**b**) thermal contraction, of different SFRMs

Table 9.6 Density of SFRM at room temperature and after exposure to 700 °C

Insulation type	Density (Kg/m^3)		Decrease in density (%)
	Room temp. (20 °C)	700 °C	
SFRM A	298	241.3	19.0
SFRM B	423.2	349.8	17.3
SFRM C	451.8	381.2	15.6

However, the loss of moisture content only account for the shrinkage phenomenon that occurs in 100–400 °C range. The intermediate expansion resulting in increase in thermal strains in 400–800 °C range is dictated by the expansion of intumescent material, such as, vermulite, which is added to SFRM to counteract shrinkage and the percentage of Vermiculite in SFRM has major influence on the level of contraction.

The change in density for three types of SFRM at ambient conditions and after exposure to 700 °C is presented in Table 9.6 [114]. There is a decrease in density in all three types of SFRM at 700 °C, which is predominantly due to the loss of moisture. This decrease in density in SFRM is comparable to that in gypsum, and attributed to dehydration reactions, which takes place with increase in temperature [115].

Other Miscellaneous Materials

Further information is available from the literature on the dilatometric and thermogravimetric behavior, apparent specific heat, and thermal conductivity of a number of materials in Group I, including asbestos cement board, expanded plastic insulating boards, mineral fiber fireproofing, arborite, and glass-reinforced cement board [7]. The properties of plastics and their behavior in fire are discussed in other chapters of this handbook and in Harmathy [2].

Summary

The use of numerical methods for the calculation of the fire resistance of various structural members is gaining acceptance. One of the main inputs needed in these models is the material properties at elevated temperatures. The thermal and mechanical properties of most materials change substantially within the temperature range associated with building fires.

Even to date, there is lack of adequate knowledge of the behavior of many building materials at elevated temperatures. Although there is sufficient information available for some materials, such as normal-strength concrete and steel, there is a complete lack of information on certain properties for widely used materials, such as wood, insulation, and so on. Often, traditional materials are being modified (e.g., high-strength concrete) to enhance their properties at room temperatures without giving due consideration to elevated temperatures. In many cases, these modifications will cause the properties to deteriorate at elevated temperatures and introduce additional complexities, such as spalling in HSC.

In the field of fire science, applied materials research faces numerous difficulties. At elevated temperatures, many building materials undergo physicochemical changes. Most of the properties are temperature dependent and sensitive to testing method parameters such as heating rate, strain rate, temperature gradient, and so on. One positive note is that in the last two decades, there has been significant progress in developing measurement techniques and commercial instruments for measuring the properties. This will likely lead to further research in establishing material properties.

The review on material properties provided in this chapter is a broad outline of the available information. Additional details related to specific conditions on which these properties are developed can be found in cited references. Also, when using the material properties presented in this chapter, due consideration should be given to the material composition and other characteristics, such as fire and loading, because the properties at elevated temperatures depend on a number of factors.

Disclaimer Certain commercial products are identified in this paper in order to adequately specify the experimental procedure. In no case does such identification imply

recommendations or endorsement by the authors, nor does it imply that the product or material identified is the best available for the purpose.

Nomenclature

a	Material constant, dimensionless
b	Constant, characteristic of pore geometry, dimensionless
c	Specific heat ($J \cdot kg^{-1} \cdot K^{-1}$)
$\overline{c}$	Specific heat for a mixture of reactants and solid products ($J \cdot kg^{-1} \cdot K^{-1}$)
E	Modulus of elasticity (Pa)
h	Enthalpy ($J \cdot kg^{-1}$)
Δh	Latent heat associated with a "reaction" ($J \cdot kg^{-1}$)
ΔH_c	Activation energy for creep ($J \cdot kmol^{-1}$)
k	Thermal conductivity ($W \cdot m^{-1} \cdot K^{-1}$)
L_v	Heat of gasification of wood
ℓ	Dimension (m)
$\Delta \ell$	$\ell - \ell_0$
m	Exponent, dimensionless
M	Mass (kg)
n	Material constant, dimensionless
P	Porosity ($m^3 \cdot m^{-3}$)
q_n	Net heat flux to char front
R	Gas constant (8315 $J \cdot kmol^{-1} \cdot K^{-1}$)
S	Specific surface area ($m^2.m^{-3}$)
t	Time (h)
T	Temperature (K or °C)
v	Volume fraction ($m^{-3}.m^3$)
w	Mass fraction ($kg \cdot kg^{-1}$)
Z	Zener-Hollomon parameter (h^{-1})

Greek Letters

α	Thermal diffusivity
β	Coefficient of linear thermal expansion ($m \cdot m^{-1}$)
γ	Expression defined by Equation 9.3, dimensionless
β_0	Charring rate (mm/min)
δ	Characteristic pore size (m)
ε	Emissivity of pores, dimensionless
ε	Strain (deformation) ($m \cdot m^{-1}$)
ε_{t0}	Creep parameter ($m \cdot m^{-1}$)
$\dot{\varepsilon}_{ts}$	Rate of secondary creep ($m.m^{-1} \cdot h^{-1}$)
θ	Temperature-compensated time (h)
ξ	Reaction progress variable, dimensionless
π	Material property (any)
ρ	Density ($kg \cdot m^{-3}$)
σ	Stress; strength (Pa)
σ	Stefan-Boltzmann constant (5.67×10^{-8} $W \cdot m^{-2} \cdot K^{-4}$)

Subscripts

g	Glass transient (temperature)
a	Of air
I	Of the ith constituent
p	At constant pressure
s	Of the solid matrix
t	True
t	Time-dependent (creep)
T	At temperature T
u	Ultimate
y	Yield
0	Original value, at reference temperature

References

1. T.Z. Harmathy, *Technical Paper No. 242,* National Research Council of Canada, Ottawa (1967).
2. T.Z. Harmathy, *Fire Safety Design and Concrete,* Longman Scientific and Technical, Harlow, UK (1993).
3. D.A.G. Bruggeman, *Physik. Zeitschr.,* 37, p. 906 (1936).
4. R.L. Hamilton and O.K. Crosser, *Industrial & Engineering Chemistry Fundamentals,* 7, p. 187 (1962).
5. J.C. Maxwell, *A Treatise on Electricity and Magnetism,* 3rd ed., 1, Clarendon Press, Oxford, UK (1904).
6. T.Z. Harmathy, *Journal of Materials,* 5, p. 47 (1970).
7. T.Z. Harmathy, *DBR Paper No. 1080, NRCC 20956,* National Research Council of Canada, Ottawa (1983).
8. V.K.R. Kodur and M.M.S. Dwaikat, "Effect of high temperature creep on fire response of restrained steel beams", J. of Materials and Structures, 43, 10, pp. 1327–1341 (2010)
9. J.E. Dorn, *Journal of the Mechanics and Physics of Solids,* 3, p. 85 (1954).
10. T.Z. Harmathy, in *ASTM STP422,* American Society for Testing and Materials, Philadelphia (1967).
11. T.Z. Harmathy, "Trans. Am. Soc. Mech. Eng.," *Journal of Basic Engineering,* 89, p. 496 (1967).

12. C. Zener and J.H. Hollomon, *Journal of Applied Physics,* 15, p. 22 (1944).
13. F.H. Wittmann (ed.), *Fundamental Research on Creep and Shrinkage of Concrete,* Martinus Nijhoff, The Hague, Netherlands (1982).
14. Y. Anderberg and S. Thelandersson, *Bulletin 54,* Lund Institute of Technology, Lund, Sweden (1976).
15. U. Schneider, *Fire and Materials,* 1, p. 103 (1976).
16. T.Z. Harmathy, *Journal of the American Concrete Institute,* 65, 959 (1968).
17. *951 Thermogravimetric Analyzer (TGA),* DuPont Instruments, Wilmington, DE (1977).
18. T.T. Lie and V.K.R. Kodur, "Thermal and Mechanical Properties of Steel Fibre-Reinforced Concrete at Elevated Temperatures," *Canadian Journal of Civil Engineering,* 23, p. 4 (1996).
19. ASTM Test Method C135 ± 86, *2007 Annual Book of ASTM Standards,* 15.01, American Society for Testing and Materials, Philadelphia (2007).
20. T.Z. Harmathy and L.W. Allen, *Journal of the American Concrete Institute,* 70, p. 132 (1973).
21. *910 Differential Scanning Calorimeter (DSC),* DuPont Instruments, Wilmington, DE (1977).
22. J.H. Perry (ed.), *Chemical Engineers' Handbook,* 3rd ed., McGraw-Hill, New York (1950).
23. W. Eitel, *Thermochemical Methods in Silicate Investigation,* Rutgers University, New Brunswick, Canada (1952).
24. T.Z. Harmathy, *Industrial & Engineering Chemistry Fundamentals,* 8, p. 92 (1969).
25. D.A. DeVries, in *Problems Relating to Thermal Conductivity,* Bulletin de l'Institut International du Froid, Annexe 1952–1, Louvain, Belgique, p. 115 (1952).
26. W.D. Kingery, *Introduction to Ceramics,* John Wiley and Sons, New York (1960).
27. T.T. Lie and V.K.R. Kodur, "Thermal Properties of Fibre-Reinforced Concrete at Elevated Temperatures," *IR 683,* IRC, National Research Council of Canada, Ottawa (1995).
28. *Thermal Conductivity Meter (TC-31), Instruction Manual,* Kyoto Electronics Manufacturing Co. Ltd., Tokyo, Japan (1993).
29. ASCE, "Structural Fire Protection: Manual of Practice," No. 78, American Society of Civil Engineers, New York (1993).
30. L.T. Phan, "Fire Performance of High-Strength Concrete: A Report of the State-of-the-Art," National Institute of Standards and Technology, Gaithersburg, MD (1996).
31. U. Danielsen, "Marine Concrete Structures Exposed to Hydrocarbon Fires," Report, SINTEF—The Norwegian Fire Research Institute, Trondheim, Norway (1997).
32. V.K.R. Kodur and M.A. Sultan, "Structural Behaviour of High Strength Concrete Columns Exposed to Fire," *Proceedings, International Symposium on High Performance and Reactive Powder Concrete,* Concrete Canada, Sherbrooke, Canada (1998).
33. U. Diederichs, U.M. Jumppanen, and U. Schneider, "High Temperature Properties and Spalling Behaviour of High Strength Concrete," in *Proceedings of Fourth Weimar Workshop on High Performance Concrete,* HAB, Weimar, Germany (1995).
34. Y. Anderberg, "Spalling Phenomenon of HPC and OC," in *International Workshop on Fire Performance of High Strength Concrete, NIST SP 919,* NIST, Gaithersburg, MD (1997).
35. Z.P. Bazant, "Analysis of Pore Pressure, Thermal Stress and Fracture in Rapidly Heated Concrete," in *International Workshop on Fire Performance of High Strength Concrete, NIST SP 919,* NIST, Gaithersburg, MD (1997).
36. A.N. Noumowe, P. Clastres, G. Debicki, and J.-L. Costaz, "Thermal Stresses and Water Vapor Pressure of High Performance Concrete at High Temperature," *Proceedings, Fourth International Symposium on Utilization of High-Strength/High-Performance Concrete,* Paris, France (1996).
37. J.A. Purkiss, *Fire Safety Engineering Design of Structures,* Butterworth Heinemann, Bodmin, Cornwall, UK (1996).
38. E.L. Schaffer, "Charring Rate of Selected Woods—Transverse to Grain," *FPL 69,* U.S. Department of Agriculture, Forest Service, Forest Products Laboratory, Madison, WI (1967).
39. B.F.W. Rogowski, "Charring of Timber in Fire Tests," in *Symposium No. 3 Fire and Structural Use of Timber in Buildings,* HMSO, London (1969).
40. N. Bénichou and M.A. Sultan, "Fire Resistance of Lightweight Wood Frame Assemblies: State-of-the-Art Report," *IR 776,* IRC, National Research Council of Canada, Ottawa (1999).
41. S. Hadvig, *Charring of Wood in Building Fires—Practice, Theory, Instrumentation, Measurements,* Laboratory of Heating and Air-Conditioning, Technical University of Denmark, Lyngby, Denmark (1981).
42. E. Mikkola, "Charring of Wood," *Report 689,* Fire Technology Laboratory, Technical Research Centre of Finland, Espoo (1990).
43. *Guide for Determining the Fire Endurance of Concrete Elements, ACI-216–89,* American Concrete Institute, Detroit, MI (1989).
44. I.D. Bennetts, *Report No. MRL/PS23/81/001,* BHP Melbourne Research Laboratories, Clayton, Australia (1981).
45. U. Schneider (ed.), *Properties of Materials at High Temperatures—Concrete,* Kassel University, Kassel, Germany (1985).
46. Y. Anderberg (ed.), *Properties of Materials at High Temperatures—Steel,* Lund University, Lund, Sweden (1983).
47. F. Birch and H. Clark, *American Journal of Science,* 238, p. 542 (1940).
48. T.Z. Harmathy and W.W. Stanzak, in *ASTM STP464,* American Society for Testing and Materials, Philadelphia (1970).

49. Y. Anderberg, "Mechanical Properties of Reinforcing Steel at Elevated Temperatures," *Tekniska Meddelande,* 36, Sweden (1978).
50. "European Recommendations for the Fire Safety of Steel Structures," *European Convention for Construction Steelwork, Tech. Comm. 3,* Elsevier, New York (1983).
51. Eurocode 3, Design of steel structures, Part 1-2: General rules-structural fire design, Document CEN, European Committee for Standardization, UK (2005).
52. T. Twilt, "Stress-Strain Relationships of Reinforcing Structural Steel at Elevated Temperatures, Analysis of Various Options and European Proposal," *TNO-Rep. BI-91-015,* TNO Build. and Constr. Res., Delft, Netherlands (1991).
53. K.W. Poh, "General Stress-Strain Equation," *ASCE Journal of Materials in Civil Engineering,* Dec. (1997).
54. K.W. Poh, "Stress-Strain-Temperature Relationship for Structural Steel," *ASCE Journal of Materials in Civil Engineering*, Oct. (2001).
55. J.T. Gerlich, P.C.R. Collier, and A.H. Buchanan, "Design of Light Steel-Framed Walls for Fire Resistance," *Fire and Materials,* 20, 2 (1996).
56. G.Q. Li, S.C. Jiang, and Y.Z. Yin, "Experimental studies on the properties of constructional steel at elevated temperatures." J. Struct. Eng., 129, 12, pp. 1717–1721 (2003).
57. BS 5950, "Structural Use of Steelwork in Building," Part 8, in *Code of Practice for Fire Resistant Design,* British Standards Institution, London (2003).
58. W. Wang, L. Bing and V.K.R. Kodur, "Effect of temperature on strength and elastic modulus of high strength steel", in Press: ASCE Journal of Materials in Civil Engineering, pp. 1–24 (2012).
59. V.K.R. Kodur and W. Khaliq, "Effect of temperature on thermal and mechanical properties of steel bolts", ASCE Journal of Materials in Civil Engineering, 24, 6, pp. 765–774 (2012).
60. J.T. Gerlich, "Design of Loadbearing Light Steel Frame Walls for Fire Resistance," Fire Engineering Research Report 95/3, University of Canterbury, New Zealand (1995).
61. P. Makelainen and K. Miller, *Mechanical Properties of Cold-Formed Galvanized Sheet Steel Z32 at Elevated Temperatures,* Helsinki University of Technology, Finland (1983).
62. F. Alfawakhiri, M.A. Sultan, and D.H. MacKinnon, "Fire Resistance of Loadbearing Steel-Stud Walls Protected with Gypsum Board: A Review," *Fire Technology,* 35, 4 (1999).
63. T.Z. Harmathy and J.E. Berndt, *Journal of the American Concrete Institute,* 63, p. 93 (1966).
64. C.R. Cruz, *Journal, PCA Research and Development Laboratories,* 8, p. 37 (1966).
65. M.S. Abrams, in *ACI SP 25,* American Concrete Institute, Detroit, MI (1971).
66. C.R. Cruz, *Journal, PCA Research and Development Laboratories,* 10, p. 36 (1968).
67. J.C. MareÂchal, in *ACI SP 34,* American Concrete Institute, Detroit, MI (1972).
68. H. Gross, *Nuclear Engineering and Design,* 32, p. 129 (1975).
69. U. Schneider, U. Diedrichs, W. Rosenberger, and R. Weiss, *Sonderforschungsbereich 148,* Arbeitsbericht 1978–1980, Teil II, B 3, Technical University of Braunschweig, Germany (1980).
70. U. Diederichs and U. Schneider, "Bond Strength at High Temperatures," *Magazine of Concrete Research,* 33, 115, pp. 75–84 (1981).
71. V.K.R. Kodur, "Fibre-Reinforced Concrete for Enhancing the Structural Fire Resistance of Columns," ACI-SP (2000).
72. A. Bilodeau, V.M. Malhotra, and G.C. Hoff, "Hydrocarbon Fire Resistance of High Strength Normal Weight and Light Weight Concrete Incorporating Polypropylene Fibres," in *Proceedings, International Symposium on High Performance and Reactive Powder Concrete,* Sherbrooke, Canada (1998).
73. V.K.R. Kodur and T.T. Lie, "Fire Resistance of Fibre-Reinforced Concrete," in *Fibre Reinforced Concrete: Present and the Future,* Canadian Society of Civil Engineers, Montreal (1997).
74. U.-M. Jumppanen, U. Diederichs, and K. Heinrichsmeyer, "Materials Properties of F-Concrete at High Temperatures," *VTT Research Report No. 452,* Technical Research Centre of Finland, Espoo (1986).
75. J.A. Purkiss, "Steel Fibre-Reinforced Concrete at Elevated Temperatures," *International Journal of Cement Composites and Light Weight Concrete,* 6, 3 (1984).
76. T.T. Lie and V.K.R. Kodur, "Effect of Temperature on Thermal and Mechanical Properties of Steel Fibre-Reinforced Concrete," *IR 695, IRC,* National Research Council of Canada, Ottawa (1995).
77. V.K.R. Kodur and R. McGrath, "Effect of Silica Fume and Confinement on Fire Performance of High Strength Concrete Columns," *Canadian Journal of Civil Engineering*, p. 24 (2006).
78. F.P. Cheng, V.K.R. Kodur, and T.C. Wang, "Stress-Strain Curves for High Strength Concrete at Elevated Temperatures," *ASCE Journal of Materials Engineering*, 16, 1, pp. 84–90 (2004).
79. V.K.R. Kodur, T.C. Wang, and F.P. Cheng, "Predicting the Fire Resistance Behaviour of High Strength Concrete Columns," *Cements and Concrete Composites Journal*, 26, 2, pp. 141–153 (2003).
80. V.K.R. Kodur and M.A. Sultan, "Thermal Properties of High Strength Concrete at Elevated Temperatures," *CANMET-ACI-JCI International Conference, ACI SP-170,* Tokushima, Japan, American Concrete Institute, Detroit, MI (1998).
81. V.K.R. Kodur and M.A. Sultan, "Effect of Temperature on Thermal Properties of High Strength

Concrete," *ASCE Journal of Materials in Civil Engineering*, 15, 8, pp. 101–108 (2003).
82. V.K.R. Kodur and W. Khaliq, "Effect of temperature on thermal properties of different types of high strength concrete", ASCE Journal of Materials in Civil Engineering, 23, 6, pp. 793–801 (2011).
83. V.K.R. Kodur, "Spalling in High Strength Concrete Exposed to Fire—Concerns, Causes, Critical Parameters and Cures," in *Proceedings: ASCE Structures Congress,* Philadelphia (2000).
84. V.K.R. Kodur, "Guidelines for Fire Resistance Design of High Strength Concrete Columns," *Journal of Fire Protection Engineering*, 15, 2, pp. 93–106 (2005).
85. J.W. McBurney and C.E. Lovewell, *ASTM—Proceedings of the Thirty-Sixth Annual Meeting,* Vol. 33 (II), American Society for Testing and Materials, Detroit, MI, p. 636 (1933).
86. *Wood Handbook: Wood as an Engineering Material,* Agriculture Handbook No. 72, Forest Products Laboratory, U.S. Government Printing Office, Washington, DC (1974).
87. C.C. Gerhards, *Wood & Fiber,* 14, p. 4 (1981).
88. E.L. Schaffer, *Wood & Fiber,* 9, p. 145 (1977).
89. E.L. Schaffer, *Research Paper FPL 450,* U.S. Department of Agriculture, Forest Products Lab., Madison, WI (1984).
90. "Structural Fire Design," Part 1.2, in *Eurocode 5,* CEN, Brussels, Belgium (1995).
91. F.F. Wangaard, Section 29, in *Engineering Materials Handbook (*C.L. Mantell, ed.), McGraw-Hill, New York (1958).
92. V.K.R. Kodur, J. Fike, R. Fike, and M. Tabaddoor, "Factors governing fire resistance of engineered wood I-joists", Proceedings of the Seventh International Conference on Structures in Fire, Zurich, Switzerland, pp. 417–426 (2012).
93. V.K.R. Kodur and D. Baingo, "Fire Resistance of FRP Reinforced Concrete Slabs," *IR 758,* IRC, National Research Council of Canada, Ottawa (1998).
94. V.K.R. Kodur, "Fire Resistance Requirements for FRP Structural Members," *Proceedings—Vol I, 1999 CSCE Annual Conference,* Canadian Society of Civil Engineers, Regina, Saskatchewan (1999).
95. T.S. Gates, "Effects of Elevated Temperature on the Viscoelastic Modeling of Graphite/Polymeric Composites," *NASA Technical Memorandum 104160,* NASA, Langley Research Center, Hampton, VA (1991).
96. Y.C. Wang and V.K.R. Kodur, "Variation of Strength and Stiffness of Fibre Reinforced Polymer Reinforcing Bars with Temperature," *Cement and Concrete Composites*, 27, pp. 864–874 (2005).
97. SK. Foster, "High Temperature Residual Performance of Externally-Bonded FRP Systems for Concrete," *MSc Thesis*, Kingston, Canada, Department of Civil Engineering, Queen's University (2006).
98. A. Katz and N. Berman, "Modeling the Effect of High Temperature on the Bond of FRP Reinforcing Bars to Concrete," *Cement and Concrete Composites Journal*, 22, pp. 433–443 (2000).
99. A. Katz, N. Berman, and L.C. Bank, "Effect of High Temperature on the Bond Strength of FRP Rebars," *Journal of Composites for Construction,* 3, 2, pp. 73–81 (1999).
100. A. Sumida, T. Fujisaki, K. Watanabe, and T. Kato, "Heat Resistance of Continuous Fiber Reinforced Plastic Rods," *Proceedings, Fifth Annual Symposium on Fibre-Reinforced-Plastic Reinforcement for Concrete Structures*, Thomas Telford, London, pp. 557–565 (2001).
101. N. Galati, B. Vollintine, A. Nanni, L.R. Dharani, and M.A. Aiello, "Thermal Effects on Bond Between FRP Rebars and Concrete," *Proceedings, Advanced Polymer Composites for Structural Applications in Construction,* Woodhead Publishing Ltd., Cambridge, UK, pp. 501–508 (2004).
102. V.R. Kodur, L.A. Bisby, and M.F. Green, "Experimental Evaluation of the Fire Behavior of Fibre-Reinforced-Polymer-Strengthened Reinforced Concrete Columns," *Fire Safety Journal, 41, 7, pp. 547–557* (2005).
103. V.R. Kodur and L.A. Bisby, "Evaluation of Fire Endurance of Concrete Slabs Reinforced with FRP Bars," *ASCE Journal of Structural Engineering*, 131, 1, pp. 34–43 (2005).
104. Y.C. Wang, P.M.H. Wong, and V.K.R. Kodur, "An Experimental Study of Mechanical Properties of FRP and Steel Reinforcing Bars at Elevated Temperatures," *Composite Structures*, 80, 1, pp. 131–140 (2007).
105. B. Yu, and V.K.R. Kodur, "Effect of Temperature on Strength and Stiffness Properties of Near-Surface Mounted FRP Reinforcement," *Journal of Composites*, Part B: Engineering, 58, pp. 510–517 (2014).
106. T.Z. Harmathy, in *ASTM STP301,* American Society for Testing and Materials, Philadelphia (1961).
107. R.R. West and W.J. Sutton, *Journal of the American Ceramic Society,* 37, p. 221 (1954).
108. P. Ljunggren, *Journal of the American Ceramic Society,* 43, p. 227 (1960).
109. M.A. Sultan, "A Model for Predicting Heat Transfer Through Noninsulated Unloaded Steel-Stud Gypsum Board Wall Assemblies Exposed to Fire," *Fire Technology,* 32, 3 (1996).
110. "Gypsum Board: Typical Mechanical and Physical Properties," *GA-235–98,* Gypsum Association, Washington, DC (1998).

111. M.A. Sultan, "Effect of Insulation in the Wall Cavity on the Fire Resistance Rating of Full-Scale Asymmetrical (1 × 2) Gypsum Board Protected Wall Assemblies," in *Proceedings of the International Conference on Fire Research and Engineering, Orlando, FL,* SFPE, Boston (1995).
112. A.H. Buchanan, *Structural Design for Fire Safety*, John Wiley & Sons Ltd., Chichester, UK (2002).
113. V.K.R. Kodur, M. Dwaikat and R. Fike, "High-temperature properties of steel for fire resistance modeling of structures," Journal of Materials in Civil Engineering, 22, 5, pp. 423–434 (2010).
114. V.K.R. Kodur and A. Shakya, "Effect of temperature on thermal properties of fire insulation", *Fire Safety Journal*, 61, pp. 314–323 (2013).
115. S. Park, S.L. Manzello, D.P. Bentz, and T. Mizukami, "Determining thermal properties of gypsum board at elevated temperatures", Fire and Materials (2009).

V.K.R. Kodur is a Professor in the department of Civil and Environmental Engineering and also serves as Director of the Center on Structural Fire Safety and Diagnostics at the Michigan State University (MSU). Dr. Kodur's research has focused on the evaluation of fire resistance of structural systems through large scale fire experiments and numerical modelling; characterization of materials under high temperature; and non-linear design and analysis of structural systems. He is a Fellow of the Canadian Academy of Engineering, a Foreign Fellow of Indian National Academy of Engineering and Fellow of ASCE, ACI and SEI. He is an Associate Editor of Journal of Structural Engineering, Chairman of ACI Fire Protection Committee, and Chairman of ASCE-29 (Fire) Standards Committee.

T.Z. Harmathy was head of the Fire Research Section, Institute of Research in Construction, National Research Council of Canada, until his retirement in 1988. His research centered on materials science and the spread potential of compartment fires.